2007

Methods to improve bond on FRP wrapped piles

Andy Schrader
University of South Florida

Methods to Improve Bond on FRP Wrapped Piles

by

Andy Schrader

A thesis submitted in partial fulfillment
of the requirements for the degree of
Master of Science in Civil Engineering
Department of Civil and Environmental Engineering
College of Engineering
University of South Florida

Major Professor: A.G. Mullins, Ph.D.
Rajan Sen. Ph.D.
Abla Zayed. Ph.D.

Date of Approval:
March 23, 2007

Keywords: carbon fiber, thermography, concrete, columns, NDT

Acknowledgments

First I would like to thank TECO Energy Inc. and the Tampa Electric Company for the donation of their time and equipment. Henderson Prestress Concrete also donated materials to this project, as did Fyfe Co. LLC and Air Logistics Co.

I would also like to thank the men of the Structural Research Team at the University of South Florida, including Julio Aguilar, Dr. Mike Stokes, Dr. Rajan Sen and Dr. Gray Mullins. Danny Winters deserves special thanks for his patience and effort. Lastly I would also like to recognize my family for their support: Chris, Matt, Mom and Dad, and also Ms. N. Bear.

Table of Contents

List of Tables

List of Figures

Methods to Improve Bond on FRP Wrapped Piles

Andy Schrader

ABSTRACT

Fiber Reinforced Polymer (FRP) sheets can provide incredible structural strength while weighing only a fraction as much as steel. When applied to piles the FRP provides strengthening through both concrete confinement and tensile reinforcement. Mainly used in structural repair, its application is relatively simple in theory. However, many factors (some avoidable, some not) can interfere with the bond between FRP and concrete. When this bond is interrupted the strength of the repair becomes compromised.

This thesis examines 2 new methods of improving FRP bond to concrete piles during the time the resin is curing. These methods are compared using 3 types of testing, both nondestructive and otherwise: acoustic analysis, infrared thermography, and pull-off testing. Therefore not only FRP bond improvement techniques are compared but also the techniques for bond evaluation.

Findings have shown a definite correlation between non destructive testing and destructive pull-off testing, as well as bond improvement both above and below the waterline when a pressure bag system is used.

Chapter 1 Introduction

1.1 Overview

Unlike the military and aerospace engineering, civil engineering is often one of the last venues to utilize new technologies. Of late, computer applications, satellite-based geographic information systems (GIS), and aerospace materials have become commonplace in the industry. Recent advancements in material manufacturing in particular have allowed the use of aerospace materials in construction, combining high strength with minimal weight. The application of this technology forms the basis of this thesis.

In Florida, advanced materials like fiber reinforced polymer (FRP) are now being used to repair concrete structures after collision, enhance their capabilities for increased load conditions, and mitigate corrosion damage along the state's approximately 1,200 miles of coastline as shown in Figures 1.1 and 1.2. Given the tremendous net population growth in Florida (about 1,000 new people per day) [2] and the subsequent strain on the transportation infrastructure, many structures in need of replacement are instead now relegated to repair.

This thesis examines some of the different products available for FRP repair of concrete piles, new methods to improve their effectiveness, and modes of evaluating quality assurance. Both vacuum and pressure bag bond improvement systems are tested

to see their effect on FRP adhesion strength. The methods are then examined using acoustic analysis, thermographic analysis and pull-off testing.

1.2 Scope of Project

This thesis tested the capability of 2 distinct methods to improve the bond between FRP and substrate on concrete piles. The post-construction FRP bond was compared using 3 types of testing, including 2 nondestructive methods. A total of 7 full-scale, prestressed concrete piles were tested at the University of South Florida structural research facility as shown in Figure 1.3.

1.3 Organization of the Report

Chapter 2 lists a background on FRP systems and their uses including common sources of pile corrosion and advantages of the FRP method. It also discusses traditional means of pile repair quality assurance (QA) methods. Chapter 3 details the preparation of each pile specimen, the FRP wrap process, and the pressure bag systems used. Chapter 4 shows the four methods used in the testing process including acoustic analysis, infrared cameras, infrared probe systems, and pull-off testing. Chapter 5 discusses results of the testing comparing both NDT and pull-off methods. Their ability to locate delaminated areas as well as the extent of delamination in those areas is investigated. Statistical results of the testing are also shown. Chapter 6 discusses the conclusions of the research, examining the different analysis techniques used and comparing their precision. Recommendations for future research are also given.

Figure 1.1 Cutting Dry Sheets of FRP Prior to Placement

Figure 1.2 FRP Wrapping of Corrosion Damaged Bridge Pile

Figure 1.3 Test Piles in the Tank Awaiting FRP Wrap

Chapter 2 Background

2.1 Literature Review

Levar and Hamilton in 2003 suggested that different types of defects appear differently on infrared (IR) images due to the variation in depth. They also noted that the greater the number of layers in an FRP system, the more difficult it is to tell what sort of defect is occurring.

In addition they observed that acoustic testing could see an estimated 70-80% of the defects located using infrared thermography (IRT) [9]. In 2005 Hamilton stated that single layer wraps are best for IRT detection of debonding, and that debonded areas beneath glass fiber-reinforced polymer (GFRP) systems are more difficult to detect than in carbon fiber reinforced polymers (CFRP) [7].

In 2006 Dutta tested FRP-wrapped concrete cylinders with IRT as well as timber bridge piles. His work showed that CFRP has a greater thermal conductivity than GFRP, therefore the debonded areas will attain thermal equilibrium more quickly. He also demonstrated that the maximum temperature difference, which is the time when locating debonds with IRT is easiest, occurs immediately after heating with CFRP but some time later with GFRP [8]. Previous research has never verified nondestructive testing using IRT with subsequent, more precise destructive testing. This thesis does so, and also presents an infrared thermography system which can be produced at a fraction of the cost of traditional infrared cameras.

2.2 Use of FRP for Concrete Pile Repair

Concrete piles may require repair or strengthening for various reasons, many of which can be mitigated by the use of FRP. Vehicle collision can instantly nullify the load-bearing capacity of any structural components affected. Accidental overloading may also occur when vehicles exceeding the maximum design weight drive across the structure. Extreme weather conditions may cause damage. Even normal weather conditions in saltwater environments can eventually corrode the structure.

Concrete piles are often placed in saltwater environments like over-water bridge foundations. The salts contained in the water take on the chemical form of chlorides, which are known to cause and accompany corrosion of steel. In addition, all concrete regardless of how well it was made will contain tiny cracks. The saltwater chlorides are constantly transported into the interior of the pile through these cracks by both splashing waves and water particles in the air. For these reasons, bridge piles spend their service lives in a hostile environment. Concrete in these conditions, unless protected by a costly electrified resistance system, is doomed to corrode eventually. The only unknown is how long that will take.

When chlorides attack steel and corrosion takes place, the steel undergoes a chemical transformation. Its molecular structure spreads out into a wider configuration. The steel expands then, increasing in volume while confined inside the pile. Since concrete is inflexible the confined steel pushes and breaks its surroundings. Whole pieces of concrete will fall off the exterior, opening larger holes for chloride entry and accelerating the corrosion process [1].

When concrete is destroyed in this manner the original cross-sectional area of the pile is reduced, causing an increase in compressive stress on the remaining material. This increased stress causes a reduction in the ultimate strength of the pile. Unsafe conditions may be created, necessitating the installation of a new pile or repair of the existing one.

It is a small consolation to engineers that this type of corrosion typically occurs only in the "splash zone" on the pile. Since the corrosion process requires both oxygen and water, reinforced concrete that is permanently underwater will not corrode in this manner as quickly. Nor will concrete that is higher up on the pile, out of the reach of ocean waves. In this middle area where changing tides cover and uncover the concrete on a daily basis, the wet-dry cycle is a primary contributor to corrosion [1].

Traditionally, damaged piles have been repaired with the original components with which they were produced. Columns could be strengthened by section enlargement, where the cross section of the column is increased by simply adding additional concrete around the sides. In this type of repair, fresh low-shrinkage concrete is placed around the old concrete with a bond breaker between the two. Once the new concrete has dried sufficiently, steel ties connecting the two sections are installed in order to encourage balanced load transfer. In another type of repair steel hoops may be attached to the surface to promote lateral confinement of the pile. Costly zinc-mesh anode "life jacket" systems have also been used [3]. Recently, however, FRP repair systems have been introduced for these purposes.

An FRP system is composed of woven fiber fabric and a liquid matrix (typically epoxy or polyurethane resin) with which the fabric is saturated as shown in Figure 2.1.

For column repair, the FRP is wrapped in circular sheets around the concrete. Once the liquid matrix hardens the FRP is bonded to the concrete substrate. This allows load transfer through the FRP fibers and around the damaged area. When used in this manner, FRP can increase flexural strength by fibrous load transfer and also retain existing strength through confining action on the column.

FRP demonstrates a higher tensile strength then steel, with weight that is practically negligible. It is so light that all components of the system can be picked up and placed by hand. No machinery is required as is the case when lifting heavy steel pieces. The light weight of the materials as well as the absence of heavy machinery provide greater safety for workers during the repair process.

Materials used in FRP repairs are generally more expensive than equivalent amounts of steel and concrete. However, FRP projects on the whole are often less expensive than traditional repairs through a reduction in amounts of the time and labor required [16].

2.3 Principles and Problems

There are 3 basic steps in the application of well-bonded FRP:

1) prepare the concrete surface by smoothing sharp edges, cleaning and roughening the concrete surface as necessary as shown in Figure 2.2
2) initiate polymerization (curing) of the liquid matrix through saturation of fibers, if necessary
3) place FRP onto concrete surface and allow to cure as shown in Figure 2.3.

The watchword for FRP application is *effective bond*. A good bond between FRP and the underlying substrate is necessary to provide a path for load transfer between the structural components and to tightly confine the concrete. Without an effective bond the FRP is reduced to the role of ornamentation. It will merely be sitting on the surface. And although the repair process is simple in theory, many things can go wrong when those three basic steps are put into practice.

For example, care must be taken to ensure that the epoxy be given the proper curing environment. An unusually warm ambient temperature can cause the epoxy to cure more quickly then anticipated. If the epoxy begins curing before it is in place with the fiber sheets, fiber misalignment can occur which yields reduced strength.Incomplete epoxy saturation of the fibers also may inhibit load transfer because the fibers are not in intimate contact with each other. It may be that the edges of the pile are not smoothed enough, forcing the fibers into an awkward 90 degree bend. Or sometimes the surface is not roughed up enough, discouraging the flow of resin into the concrete [6]. With so many ways to improperly apply an FRP repair, it is apparent that sufficient surface preparation is at once both crucial and care-intensive.

Once the repair has been made, it is important to ensure its effectiveness by examining the bond between the substrate and the FRP. Traditionally the strength of this bond has been quantified with pull-off tests or acoustic testing [1]. However, pull-off tests are destructive by nature and leave an open hole in the concrete where the test was performed. Acoustic tests are subjective and of a mostly qualitative nature. Non-destructive techniques besides acoustic testing (thermal, ultrasonic) have been introduced for this purpose but have not yet gained widespread acceptance.

The difficulties involved in achieving good bond, as well as the means to ensure that a good bond has been created, represent the greatest limitations in the present technology. These two subjects are intended for improvement by the research detailed in this thesis.

Figure 2.1 Field Saturation of FRP Fibers with Curing Compound

Figure 2.2 Grinding Edges of Pile to Ease FRP Application

Figure 2.3 FRP Wrapping of Pile During Laboratory Study

Chapter 3 Experimental Procedure

3.1 Pile Setup

A total of eight 5 ft long x 12 in wide square prestressed piles were used in the study. These were obtained by cutting two 20 ft long piles into 1/4 sections as shown in Figures 3.1 and 3.2. The piles were donated by Henderson Prestress Concrete because of slight damage which made them unfit for structural support. Each was prestressed by eight 0.5 in diameter Grade 270 steel strands.

After transport back to the University of South Florida structural research facility, the edges of each pile were rounded to a ½ in radius using a grinder as shown in Figure 3.3. This would allow the FRP fibers, when wrapped around the pile, to make a smoother transition around 90 degree bends. In addition any irregularities were patched and filled with hydraulic cement. Any crack larger than hairline width was sealed with epoxy.

No information was available on the compressive strength of the concrete so a Schmidt hammer was used to determine the value as shown in Table 3.4. This device hits the concrete with a known force; the rebound created is dependent on the hardness of the concrete. This way the compressive strength can be measured in a non destructive manner. Using this method the average strength was found to be approximately 4,000 psi as shown on Table 3.1.

In order to simulate maritime conditions, the piles were placed inside a 10 ft x 6 ft x 4 ft deep tank filled with potable water. The depth of the water inside the tank was such that exactly half the wrap length (18 in) would be underwater and half (18 in) above. Accordingly, the tank was filled with water to a nominal depth of 3 ft. The piles remained stationary in these water-filled tanks for 3 months prior to testing, in order to encourage organic growth similar to that seen on in-service bridge piling.

As stated previously the surface of the concrete should be cleaned before FRP application as shown in Figure 3.5. The absence of surface contaminants allows for direct contact between the repair components. In previous projects of this nature (and the first stage of this project), a 3 ksi water pressure had been used with a standoff distance of 1 to 2 in. Due to unsatisfactory results, however, it was later determined that this pressure should be increased to 10 ksi. This increased pressure required a trailer-mounted industrial pressure washer to be brought in. It weighed approximately 3,000 pounds and had a flow rate of 14 to 16 gpm at 10 ksi.

Once the piles were properly cleaned and prepared similar to the manner of actual construction practice, they were ready to undergo the FRP application process.

3.2 FRP Wrapping

Two different FRP systems were used: Fyfe Co. LLC and Air Logistics Co. Five piles were wrapped using Air Logistics' Aquawrap ® system and 3 using Fyfe's Tyfo ® SEH-51A system. Each pile received three layers of wrap total: one layer of unidirectional glass fiber in the longitudinal direction and two unidirectional layers in the

transverse direction. This configuration is similar to that of field pile repairs: longitudinal fibers act as additional tensile reinforcement to increase flexural strength and transverse fibers confine the concrete to retain existing strength.

For both systems the longitudinal layer consisted of four 3 ft long x 1 ft wide pieces. The centerline of each longitudinal strip was centered over the chamfered edges so that the edge of the strip fell along the center of the pile.

The dimensions of the transverse pieces, shown in Figures 3.9 and 3.10, differed between systems. Air Logistics piles used a single 8 in x 52 ft long piece whereas Fyfe piles received two 3 ft x 50 in pieces. The FRP-repaired area extended 1.5 ft above and below the waterline to create a 3 ft wide repair area shown in Figure 3.20. This is similar to commonly required “splash-zone” repairs on bridge piles.

After the FRP layers were applied, multiple layers of plastic stretch-wrap were wrapped tightly around the pile. The stretch wrap is applied in order to press the FRP more tightly against the pile. The kind used in this research is typically pre-perforated. However when it is wrapped around a pile multiple times the holes get covered up by subsequent layers. Therefore it is preferable to slice additional holes through the layers of stretch-wrap to allow an exit path for air and gases created by the chemical reaction of some FRP curing processes.

After wrapping, while the FRP systems were still curing and hardening, the experimental bond-improvement systems were applied to the piles. The Air Logistics piles tested both vacuum bag and pressure bag confinement systems while the Fyfe piles tested only the pressure bag. In addition, each system utilized a control pile wrapped only

with standard stretch wrap on the FRP area and no additional confinement system. This would help to determine the effectiveness of the vacuum and pressure bags. The test matrix is summarized in Table 3.2.

The original test plan called for four piles of each system to be tested with a vacuum system. One control pile was to be used as well as three piles subjected to a confining pressure of 300 psf, 720 psf and 1440 psf. This plan had to be altered, however, because of problems associated with sealing the pile as discussed later on in this thesis.

3.3 Pressure System Details

Both the vacuum bag and pressure bag worked by applying compression to the FRP sheets and pressing them onto the substrate with a force greater than that which they would normally experience. In theory this would allow the liquid matrix and fibers to wedge more deeply into the concrete pockmarks, similar to strips of Velcro coming together. Both systems wrapped around the pile in the same manner as a blood pressure cuff for the arm. The vacuum bag utilized negative pressure to remove all air from the bag and force it to press onto the pile. The other system used positive pressure to inflate an air bladder, which would similarly induce pressure on the pile.

3.3.1 Vacuum Bagging

Vacuum bagging is a well established technique for applying FRP and is often used for commercial applications. As the name implies, vacuum bagging requires the

The essential components of the vacuum bagging system are (1) a vacuum bag and (2) a vacuum pump capable of creating a significant vacuum. Additionally, the system requires a means of soaking up expelled resin as well as removal of the resin after the FRP has cured. This is done so that the resin does not stick to the FRP and mar its appearance.

The vacuum system is shown in Figures 3.12-3.16. In this figure a porous thin film (which will not stick to the resin) is referred to as the “release” and the thicker layer of absorbent material is called a “breather.” In addition to soaking up expelled resin, the breather also allows air to be extracted from the interior of the bag. The entire system is sealed at its ends so that a vacuum can develop.

In total there are three layers of fabric in the vacuum bag system: the innermost release film, then a “breather” layer composed of burlap cloth; and last a leak-proof clear plastic sheet. Each layer has its edges taped down to ensure a tight seal.

3.3.2 Pressure Bagging

Another way to apply positive pressure to the FRP repair area is with a pressure bag. This system incorporates a low-tensile strength airtight bladder contained within a restraining structure which can be either rigid or flexible. Flexible restraints are more desirable as they can be fitted and adapted as necessary to accommodate multiple pile sizes. The restraining pressure to assure proper contact is limited to the hoop strength of the pressure bag.

The system was designed to wrap around the circumference of the pile. Its exterior utilizes a heavyweight, puncture-resistant nylon fabric which can withstand the rigors of the construction site. It measures 6'-7" high x 9'-0" wide and secures to itself using a vertical row of 21 metal clips at 2 in o.c. Inside is the air bladder which is connected to a source of compressed air. A cinch strap is attached and tightened around the top and bottom of the bag once it is placed on the pile as shown in Figure 3.12.

Shown in Figure 3.19, the bag's interior air bladder was composed of a 40 mil thickness, poly-vinyl chloride (PVC) airtight shower pan liner which conformed to ASTM D4551. This flexible sheeting, when inflated to capacity, contained the pressurized air. Once attached to the pile the positive air pressure, applied uniformly to the repair area, was either 2 psi (288 psf) or 5 psi (720 psf).

The procedure of the pressure bag application was as follows:

1) Wrap the deflated bag around all faces of the pile, attaching all toggles to ensure a snug fit
2) While holding the bag up in place, begin inflating the pressure bag by activating the air compressor
3) As the bag fills with air, manually press down on the bag to smooth out any wrinkles. This ensures that pressurized air has a free passage all the way around the pile.
4) Once the bag is inflated, tension the cinch straps at top and bottom

3.4 Air Logistics Piles Detail

The Aquawrap system uses unidirectional glass fibers. It begins curing on contact with moisture transmitted through the air or through direct contact with water. For this reason it is shipped in vacuum sealed pouches which are not opened until the concrete is ready for its application. In this system, a base resin coating is applied to the concrete surface prior to wrapping as shown in Figure 3.7. This helps to improve the concrete bond because surface defects in the concrete are filled in with the resin. This allows more of the concrete surface to contact the FRP and facilitates load transmission between the two components. In addition, the cohesive properties of the resin encourage the FRP to adhere to the pile. Two different resins were evaluated here: Air Logistics' Aquawrap Base Primer #4 (polyurethane) and Bio-Dur 563 (epoxy). These were each applied to two of the four pile surfaces.

The chemical reaction that occurs during polymerization (curing) of Aquawrap FRP produces carbon dioxide (CO_2). Therefore if it is curing underwater then gas bubbles will be produced. If the bubbles remain under the FRP material they can interfere with the bond, so they must be transported out of the system. For this reason a breathing layer was placed between the stretch wrap and the vacuum bag to allow the generated gases to escape.

Test piles A1 and A4 were wrapped on the first day. A1 functioned as the Air Logistics control pile while A4 received a vacuum pressure of 1440 psf. However an air-tight seal for pile A4's vacuum bag was achieved only with great difficulty. Extensive cracking above the FRP repair area allowed air to flow freely through the pile. This

discouraged the vacuum bag from sealing with the repair surface. After 45 minutes the air leak was contained by filling in the cracks with epoxy. The vacuum bag was finally applied after 1 hour of curing.

Piles A2 and A3 were repaired next. This time the base resin was applied to the entire pile face, well beyond the repair area, in order to seal the cracked concrete surface. As before, two surfaces used Air Logistics resin and the other two used Bio-Dur 563 epoxy.

Pile A3 received its FRP repair immediately after application of the base resin. As with pile A4, and despite the full-face resin coating, the vacuum bag had difficulties sealing with the repair surface. Eventually however an air-tight seal was achieved and a 1440 psf vacuum pressure applied to the surface.

Pile A2 was allowed to cure for 24 hours. After that time, however, the resin pre-coat was inspected and was found to have achieved no significant bond with the concrete substrate as shown in Figure 3.8. As a result no FRP was applied to the pile. This pile was then abandoned and not used for future tests.

It was concluded that vacuum bagging was only effective on piles free of full length cracks so that an air-tight seal could be obtained. A pressure bag system, by contrast, would require no air-tight seals because it relied only on external pressure. It was decided to abandon the vacuum bag system, design and then build an inflatable pressure bag system

Following this process the last Air Logistics pile (F4) was repaired using the pressure bag system to see if it would yield different results. Once again a breathing layer

was placed between the stretch wrap and the pressure bag to allow the generated gases to escape. A positive pressure of 720 psf was applied to the repair area. Gas or air bubbles generated during the curing phase were seen escaping from the top and bottom of the repair area. These were not seen during the curing phase of the vacuum bagged piles, which may indicate that the pressure bag did a better job of forcing air and CO_2 bubbles out of the system. There were no major difficulties in the application of the pressure bag, as opposed to the air leaks encountered with the vacuum bags.

3.5 Fyfe Piles Details

Following the dismissal of the vacuum bag and production of the pressure bag, Fyfe piles F1 and F2 were tested with a pressure bag while F3 served as the control pile. The Tyfo ® SEH-51A uni-directional glass fabric was impregnated with Tyfo ® SW-1 epoxy and applied to the three piles. The pressure bag applied a pressure of 720 psf and 300 psf to piles F1 and F2, respectively.

In general the pressure bag system was much easier to apply to piles than the vacuum bag system. Because of the pressure bag's own weight, however, it had a tendency to slide down the pile before it was inflated. After inflation, the pressure bag could become overly buoyant and slide in an opposite direction back up the pile. For this reason cinch straps were attached to the top and bottom of the pile. These worked to secure the bag tightly against the pile and discourage vertical displacement.

Figure 3.1 Loading Piles Onto Trailer at Henderson Prestress Yard

Figure 3.2 Cutting Piles Into 5 ft Sections

Figure 3.3 Grinding Corners of the Pile


Figure 3.4 Testing Compressive Strength with Schmidt Hammer

Figure 3.5 Pressure Washing Piles in Tank

Figure 3.6 Piles in Tank, Awaiting FRP Application

Figure 3.7 Applying Transverse FRP Layer to Fyfe Pile

Figure 3.8 Applying Resin Pre-coat
to Air Logistics Piles

Figure 3.9 Peeling Off Unbonded Resin

Figure 3.10 Applying Transverse FRP Layer to Fyfe Pile

Figure 3.11 Hammering Down Layers for Vacuum System

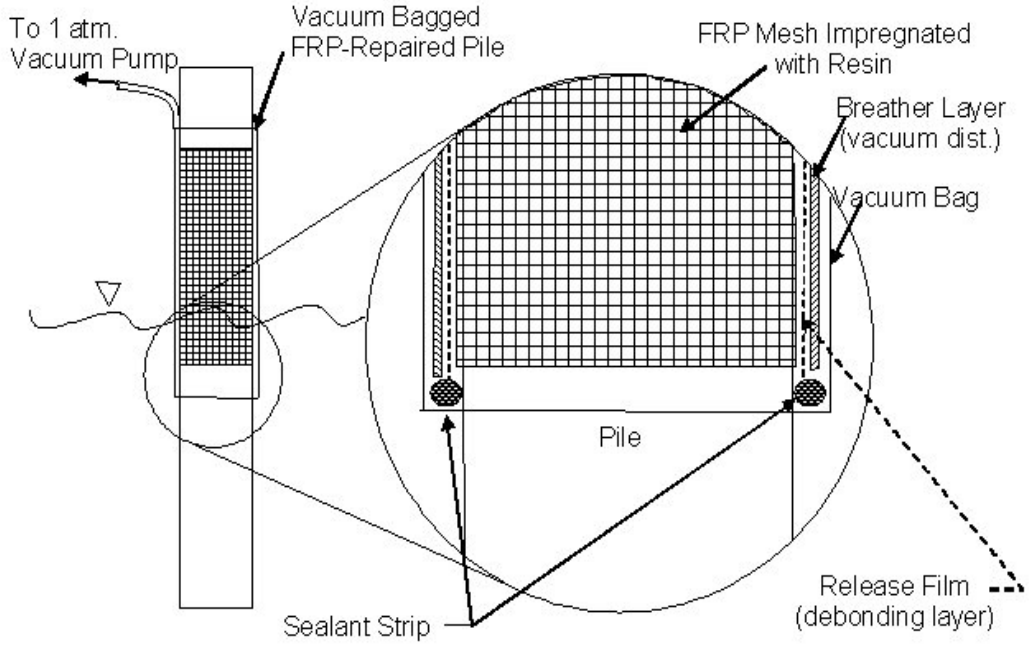

Figure 3.12 Vacuum Bag Schematic

Figure 3.13 Close-up of Vacuum Assembly

Figure 3.14 Vacuum Seal Installed, Awaiting Final Shrink Wrap Layer

Figure 3.15 Vacuum System After Final Shrink Wrap Layer Applied

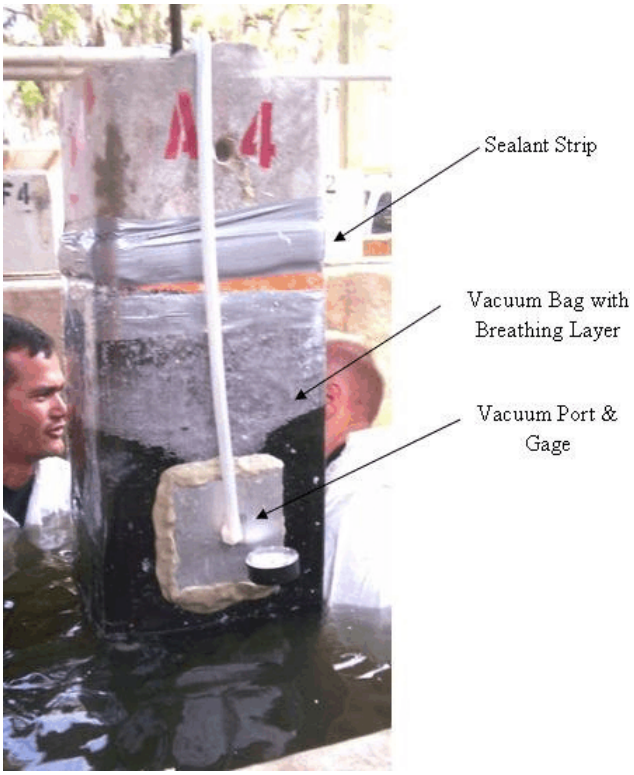

Figure 3.16 Vacuum Bag Components

Figure 3.17 Pressure Bag Shown on Pile, Inflated, with Vertical Toggle System

Figure 3.18 Pressure Bagged Fyfe and Air Logistics Piles

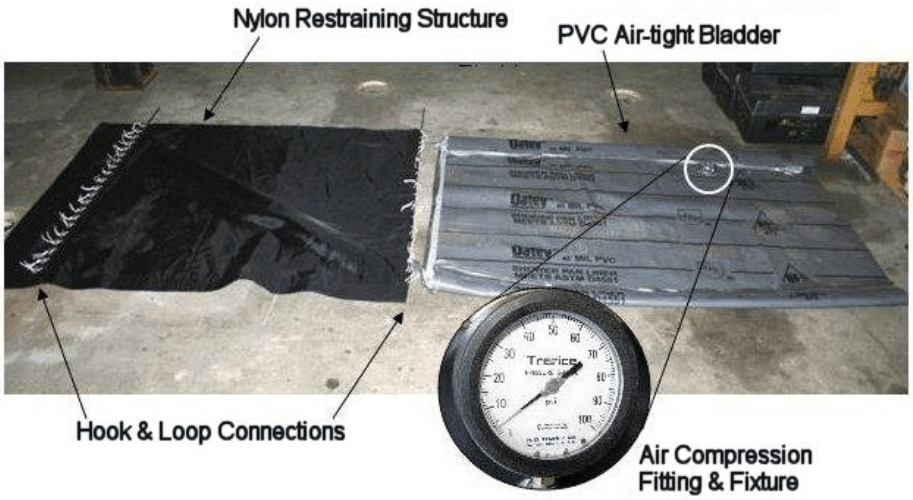

Figure 3.19 Pressure Bag Components

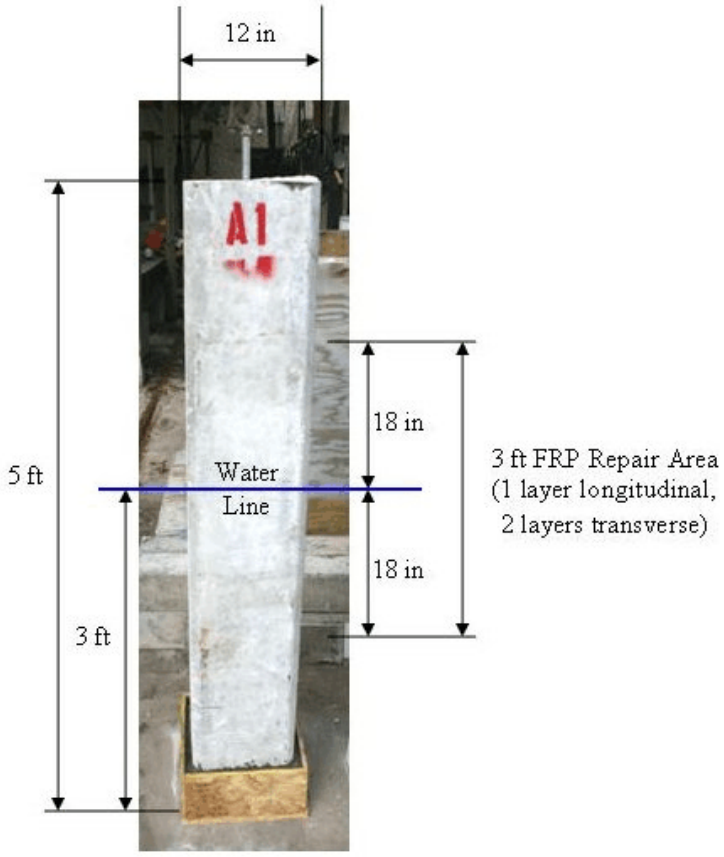

Figure 3.20 Wrap Length Details

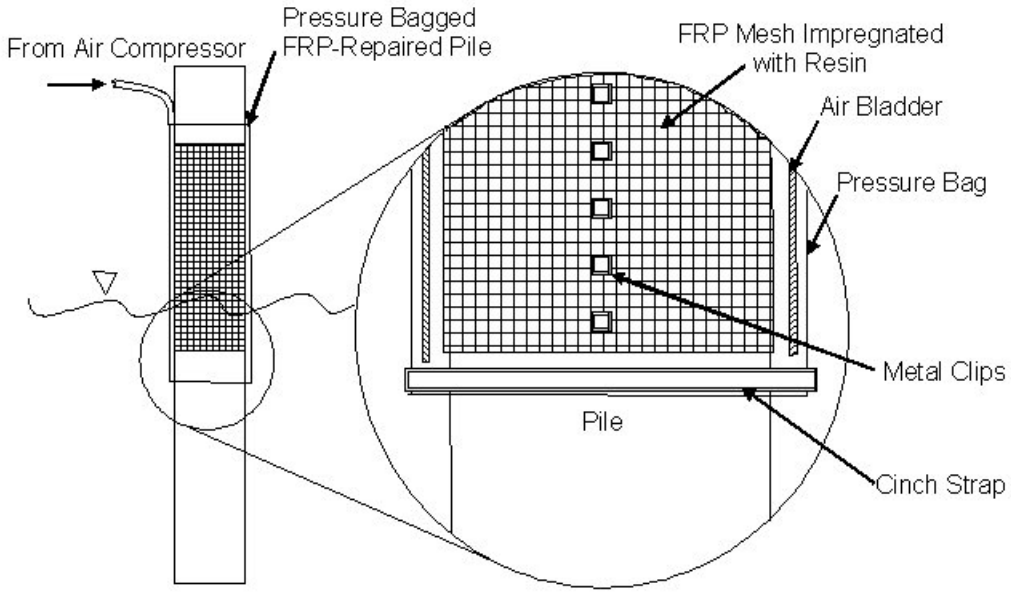

Figure 3.21 Pressure Bag Schematic

Table 3.1 Schmidt Hammer Results

Test Pile	Average f'c (psi)
A1	4133
A2	3933
A3	4144
A4	3975
F1	3850
F2	3875
F3	3975
F4	3850

Table 3.2 Test Matrix

Test Pile	Wrapping System	Confinement System	Applied Pressure (psf)
A1	Air Logistics 1 longitudinal layer, 4 pieces - 3 ft x 1 ft 2 transverse layers, 1 piece - 8 in x 52 ft	Control (stretch wrap only)	0
A2*		N/A	N/A
A3		Vacuum Bag	1440
A4		Vacuum Bag	1440
F1	Tyfo SEH-51A 1 longitudinal layer, 4 pieces - 3 ft x 1 ft 2 transverse layers, 2 pieces - 3 ft x 50 in	Pressure Bag	720
F2		Pressure Bag	302
F3		Control (stretch wrap only)	0
F4	Air Logistics (same as A1-A4 above)	Pressure Bag	1440

* Pile A2 was abandoned and not used for pressure bag tests

Chapter 4 Quality Control

4.1 Quality Control Methods

After application of the FRP using the two improvement methods, the FRP-concrete bond had to be evaluated. This was achieved in a series of tests using visual, acoustic, and thermographic analysis as well as pull-off testing. Acoustic analysis was performed first, in order to get a general idea of the bond quality. Testing of this sort is thought to be able to detect (at best) 70-80% of the poor-bond areas which more advanced NDT can find [9]. After the acoustic analysis, a thermographic analysis was performed using both FLIR digital infrared cameras and a Depth Encoder Infrared Thermocouple (DEIT) system.

The DEIT system provided a more detailed view of the areas of suspected poor bond, including the size and location of those areas. As detailed as these tests were, however, NDT can only give probable indications. It is impossible to know for certain whether FRP is bonded to the concrete or not unless it is physically removed from the substrate. For this reason, pull-off tests were performed on the faces of the piles. These tests served to validate the results of the previous nondestructive evaluations.

4.2 Acoustic Analysis

The bond strength on the lab piles was first evaluated using a nondestructive acoustic method. In this test, the surface of the FRP is struck with a rigid object. The

sound emitted can indicate whether the area underneath is debonded or not. In regions where the FRP is not in intimate contact with the substrate a hollow, ringing sound will be produced. This sound is distinct from the sound produced in areas of good bond. Although the test is simple it is fast, effective and widely used for nondestructive evaluation.

A series of 4 in x 4 in squares were drawn in a grid system on the 4 faces of each pile. The entire grid measured 40" high by 12" wide. Each grid covered the FRP-wrapped portion of each face, and began and ended at the same place each time. This way the location of possible debonds could be easily compared from face to face and possible location trends could be spotted. The area of each grid intersection was struck with a handheld solid wood shaft, and the sound compared to surrounding areas as shown in Figure 4.1

Each location was given one of three bond ratings depending on its acoustic emission. An “A” rating meant that there had been no hollow overtones detected, and the bond was thought to be satisfactory. “B” meant that hollow, higher-pitched overtones were detected and that the bond below was thought to be deficient. “C” indicated that the FRP had visibly separated from the concrete and that indications of debonding were obvious.

Although a good preliminary analysis tool, there are problems associated with this test. First, it is subjective and based on the listening and comparative ability of the testing technician. What one person hears as a definitive aural indication of debonding, another person might not notice.

Second, many areas of delamination simply don't produce the tell-tale noise associated with poor bond. It is common practice in concrete slab evaluation to assume that an additional 100% of the debonded areas (or nearly debonded areas that will also require replacement) are not recorded [7]. In addition, the acoustic analysis yields mostly qualitative information and areas of delamination must be located and recorded by hand.

4.3 Infrared Thermography (IRT) Theory

After acoustic analysis the pile faces were examined using the nondestructive technique of IRT. This is based on the theory of temperature differentials. Where FRP is well bonded to the concrete, externally applied heat energy will be able to quickly transfer down into the substrate and away from the FRP surface. Therefore the heat energy will dissipate into the pile and the surface will remain relatively cool. However if the FRP does not retain a solid interface with the substrate, heat energy will not have an efficient path to travel. It will be effectively trapped in the outermost surface layer of the FRP and the surface will remain relatively hot. To summarize, if heat is rapidly applied to a pile which possesses areas of both good and poor FRP-concrete bond, well bonded regions will dissipate heat and remain cool while poorly bonded areas will accumulate heat energy. By contrast, a pile which has been exposed only to ambient temperature may have equalized over time. Its delaminated FRP areas will display the same temperature as the surrounding concrete and will remain unobtrusive. An example of this is shown in Figures 4.16 and 4.17.

Both acoustic analysis and IRT analysis depend on the principles of energy transfer to detect anomalies. When a pile is struck with a hammer, a good bond allows the impact energy to dissipate into the pile. Only a small amount of that energy is able to be converted into noise. In the case of poor bond, however, not as much energy is able to be transferred, therefore more energy is available to create noise and the tell-tale hollow sound. Therefore both acoustic and IRT analysis should provide similar results since they are derived from similar methods.

4.3.1 IRT Analysis

A FLIR digital infrared camera was used to provide a qualitative first look at the faces. These piles had been left outside, exposed to the elements and ambient temperatures for more than 24 hours. It was attempted to photograph the piles using only the temperature differentials resulting from ambient changes as well as differentials resulting from heat energy applied with hot quartz lamps. As shown in Figures 4.13-4.15, the results suggested that suspected areas of delamination become more apparent when an external heat source is applied. It was also seen that bare concrete (specifically in the round coring hole at bottom right) appears to maintain temperature more easily than FRP-wrapped areas when a temperature differential is applied.

After that the Depth Encoder-Infrared Thermocouple (DEIT) system was used to obtain quantitative information on the size and location of the suspected areas of poor bond. This system is shown in Figures 4.8-4.12. All 7 piles were scanned by the DEIT system, which acts in a manner similar to that of a digital document scanner. It was

custom-built at the University of South Florida research facility. It uses a 500W cylindrical heat lamp which is passed over the pile at a distance of 2" in order to establish temperature differentials.

Immediately trailing the heat source is a row of 10 infrared probes which take surface temperature readings. The probes are attached to the heating element so there is a minimal lag time between surface heating and surface reading. A digital depth encoder is used to monitor the probes' movement down the face of the pile. All of these electrical components are connected to a portable data acquisition system which synchronizes the data. Everything except the data acquisition system is mounted to a mobile, vertical steel frame which can be wheeled up to the pile face. Using ball bearing attachments, the heat source and probes can smoothly scan down the face of the pile while recording information.

The heat source evenly transferred approximately 42 Joules/in^2 over the pile face while scanning. This heat application resulted in surface temperatures between approximately 90-150 °F on the FRP repair area and 80-90 °F on bare concrete.

Temperature readings coupled with position data from the depth encoder allowed the production of a contour style "map" of the pile. The width of the face was taken as the x-axis, the length of the pile was taken as the y-axis, and temperature readings were taken as the z-axis. Each probe's x-axis position remained constant throughout the test. The y-axis position varied as the probes were moved down the pile. The z-axis value also varied as the probe recorded different temperatures.

This data was transferred into Microsoft Excel and then analyzed using Excel along with software developed at the University of South Florida. This software allowed easy conversion of the raw data sets into 3-D graphics depicting the location of the suspect areas. Because the core temperature of concrete piles changes due to varying ambient temperatures, the data was normalized to permit equal comparisons of heat differentials.

The advantage of the DEIT device is that the entire pile can be scanned from a close distance, with every area of the pile face being exposed to the same amount of heat. Because the system was motorized the probes descended the pile face at a constant rate (approximately 1 in / sec) and energy (heat) transfer was uniform (approximately 42 Joules / in^2) across the face.

The emissivity of the epoxies used was investigated because Fyfe piles use an epoxy overcoat while Air Logistics piles do not. An Air Logistics pile was scanned in its original condition first and then coated with the epoxy used for Fyfe piles to see if it would show up differently on the thermal scan. The difference in thermal signatures proved to be negligible as shown in Figures 4.20 and 4.21.

4.3.2 Evolution of the DEIT System

Originally the thermal scans involved a small data acquisition device and IR probes mounted to an aluminum bar. Multiple heat lamps were placed at equidistant locations over the pile surface, allowed to heat the FRP surface for approximately 30 seconds and then removed. At this point the bar-mounted IR probes were passed over the surface by hand and readings taken.

There were inherent problems with this set-up. First, the early data acquisition device could only sample at a maximum rate of 0.5 Hz. Therefore unless the probes were moved very slowly they would miss significant amounts of data between readings. However, if the probes were moved very slowly then it would be possible for the bottom of the pile to have cooled down before the probes reached it. Therefore the temperature readings at the top of the pile would always end up being cooler than the readings at the bottom. This could incorrectly imply more extensive delamination at the top of the pile than at the bottom.

Eventually a more capable data acquisition system was used which allowed the probes to take temperature readings at a rate of 5 Hz. This would allow the probes to scan more quickly down the pile while still recording a sufficient amount of information per unit length. It was also decided to motorize the system and attach the probes to a heat source. This would ensure a constant rate of heat transfer and also take out the variable of time. With the heat source connected to (and moving at the same speed of) the probes, each area would receive the same amount of heat before scanning and the probes could move as slowly as the system required.

4.4 Pull-off Testing

For various reasons it would have been possible for the accuracy of the NDT to be flawed. Acoustic analysis, for example, is subjective and dependent on the operator. Material undulation, along with the unknown material properties of reflectivity, emissivity and absorbity could give misleading data to the IRT systems. Because of this,

pull-off tests were performed last to substantiate the NDT results. Pull-off testing typically provides consistently repeatable results regardless of the user.

The direct tension pullout bond test (ASTM D4541), or pull-off test, uses rigid disks that are affixed to a surface. This test is shown in Figures 4.1-4.4. For these tests a circular coring was made around the test area. Then that coring ring was filled in with Vasoline to keep epoxy from filling in the hole. A 1.26 in diameter aluminum disk was then epoxied to the FRP surface test area using Sikadur 32 epoxy, as shown in Figure 4.3. Once the epoxy had cured the disks were removed with an Elcometer 106 adhesion tester. This device measures the amount of force required for the disk to dislodge from the concrete. Because the disk is bonded to the FRP and the FRP is supposedly bonded to the concrete, valuable information can be obtained from the manner in which the disk is dislodged. Since the pull-off force is read directly from the adhesion tester, and the area of the disk which received the tensile stress is known, tensile stress at failure can be directly calculated using the equation *stress = force / area*.

Pull-off tests were performed on each pile both above and below the waterline if possible. However, material deformations prevented testing in certain areas as did overly weak bond strength.

The desired mode of failure for pull-off tests is for separation in the concrete. In this case the bond between the FRP and concrete is so strong that the FRP will not simply peel off the concrete. The two materials have bonded to become a single system. Therefore it is impossible to remove the FRP without pulling out concrete as well. Concrete failure indicates that the best possible bond between FRP and concrete has been achieved.

There are two types of concrete failure: full or partial failure. In a full failure, shown in Figure 4.6, concrete covers all or nearly all of the removed disk. This is preferred over a partial failure which occurs when concrete does covers only part of the disk and FRP may be seen where no concrete is present.

If the metal disk were removed with FRP attached but no concrete, it indicates that the FRP was not effectively bonded to the concrete in that area. If the disk were removed without FRP attached, it indicates a failure of the epoxy used to bond the disk to the FRP surface. Another type of failure observed which was unique to the Air Logistics piles was a “veil” failure, which occurred above the strengthening fibers of the FRP in the non-structural top layer of the fabric.

Regardless of the failure type, the amount of tensile stress recorded at failure is valuable information because it represents the minimum tensile strength of the system in that area. Typically, 200 psi adhesion strength and failure in the concrete substrate is taken as the minimum acceptable result for bond-critical FRP applications [8]. For contact-critical applications however there is no minimum adhesion strength requirement. For this research 200 psi was taken as the minimum satisfactory value.

Figure 4.1 Acoustic Analysis

Figure 4.2 Coring for Pull-off Test

Figure 4.3 Pull-off Test Area

Figure 4.4 Elcometer Attached to Dolly for Pull-off Test

Figure 4.5 FRP Failure of Pull-off Test

Figure 4.6 Full Concrete Failure of Pull-off Test

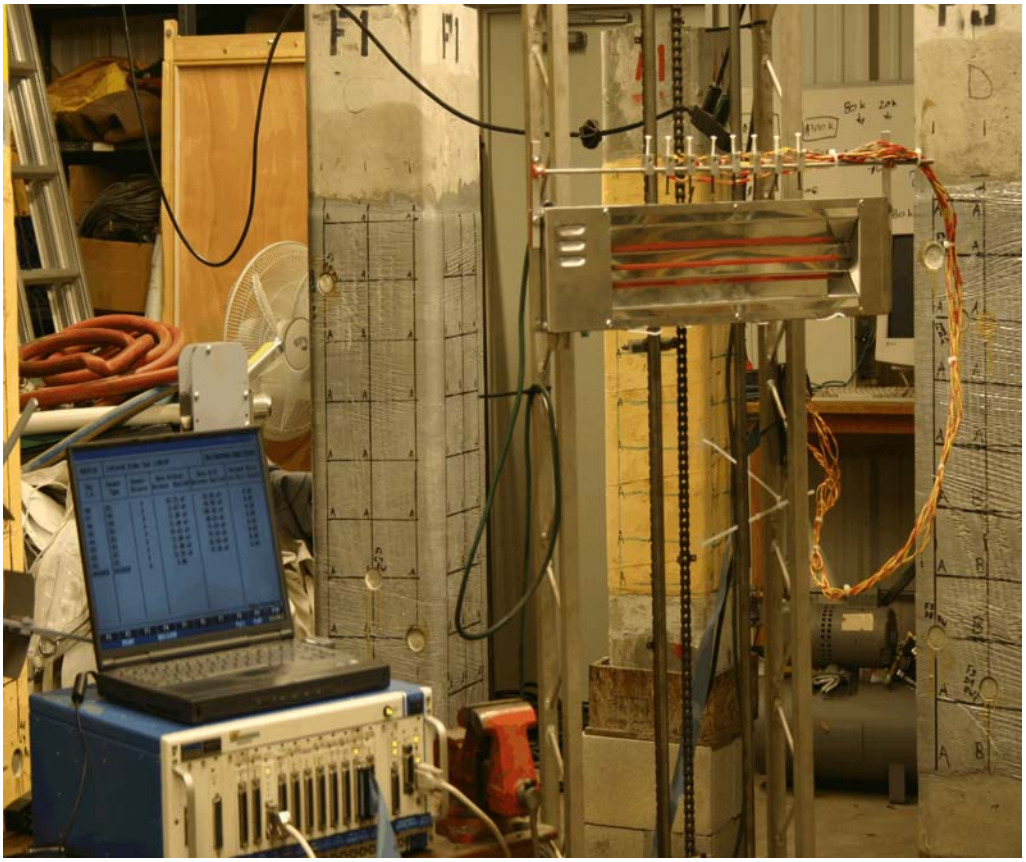

Figure 4.7 Laptop with DEIT System (Probes Were Later Replaced)

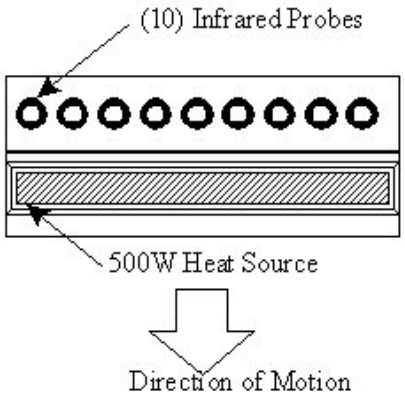

Figure 4.8 DEIT System Schematic

Figure 4.9 DEIT System Scanning a Pile

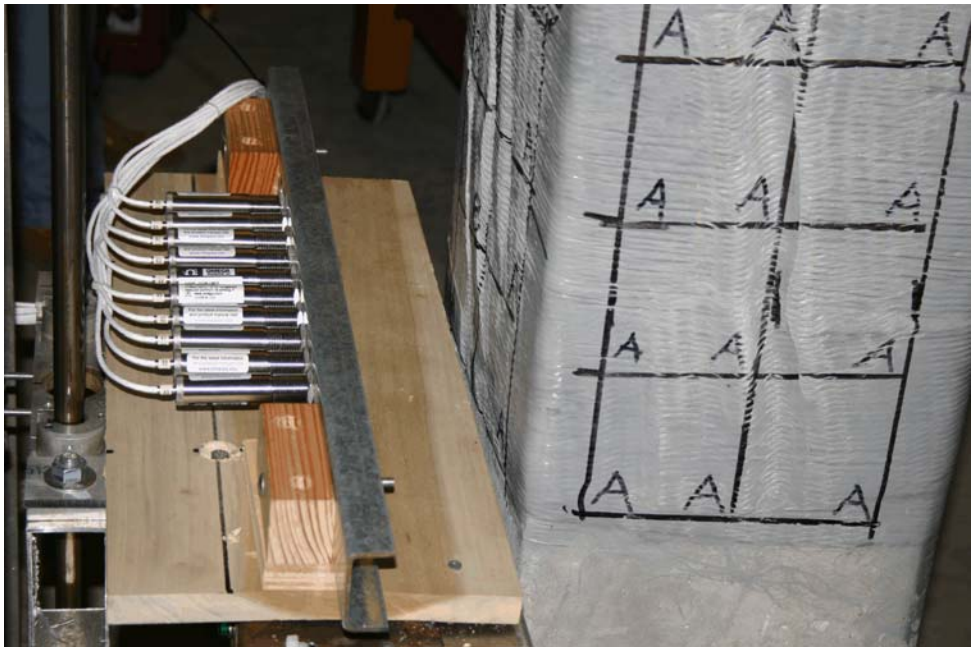

Figure 4.10 Side View of DEIT System

Figure 4.11 DEIT Motor Assembly

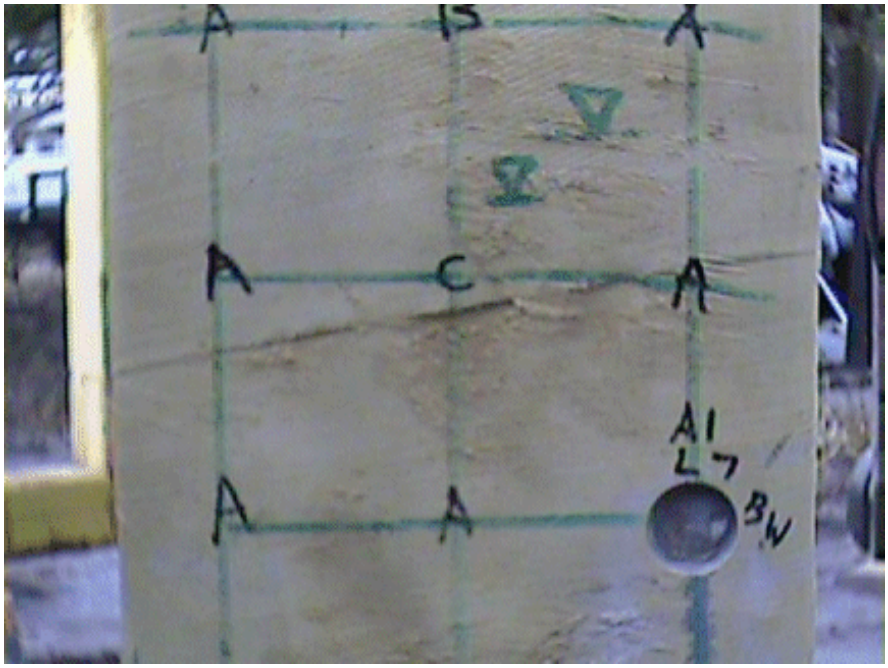

Figure 4.12 Pile Seen Under Visible Spectrum Light

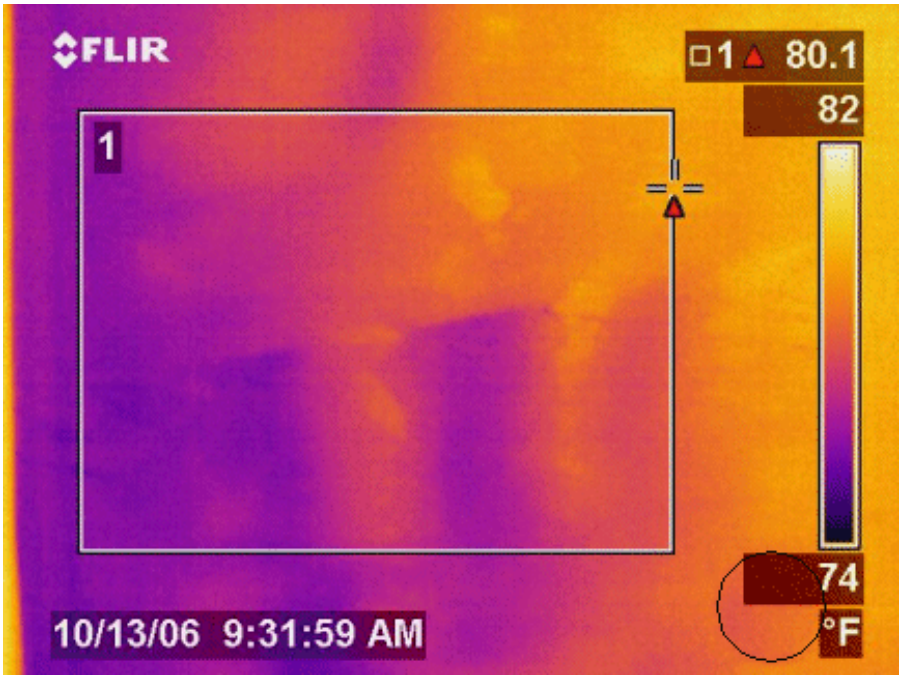

Figure 4.13 Pile Seen Under IR Light and Ambient Temperatures

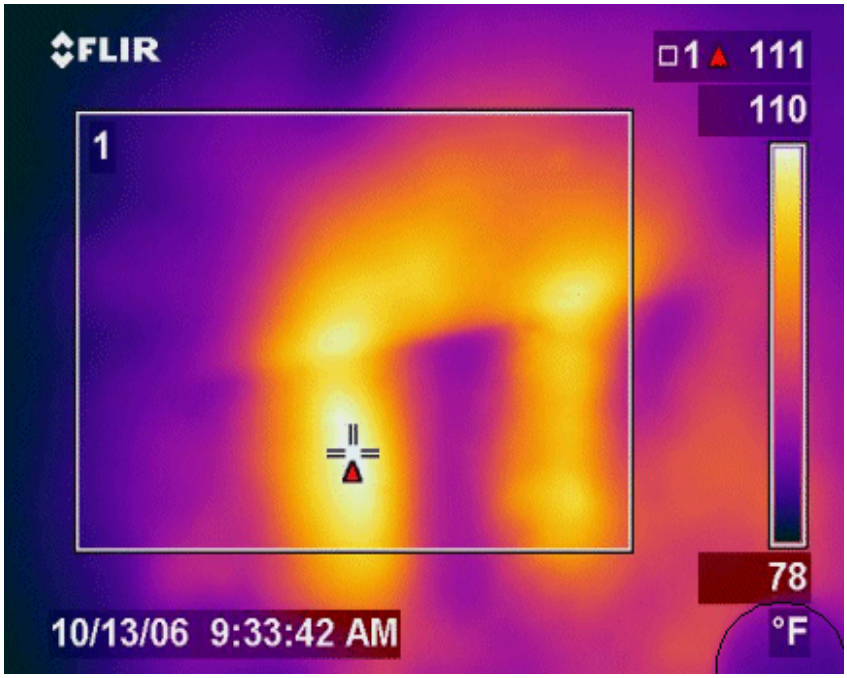

Figure 4.14 Pile Seen Under IR Light and Externally Applied Temperatures (Note Coring Hole at Lower Right)

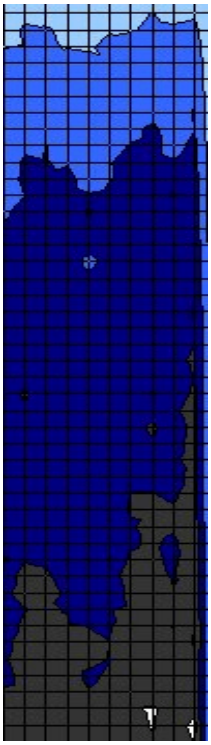

Figure 4.15
Thermal Scan Showing Differential Temperatures Using Ambient Heat

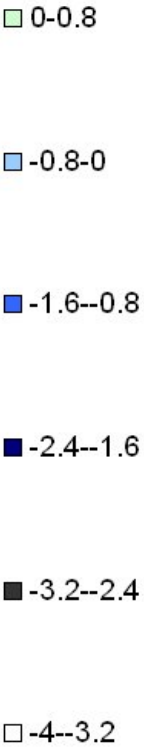

Figure 4.16
Ambient Differential Legend (°F)

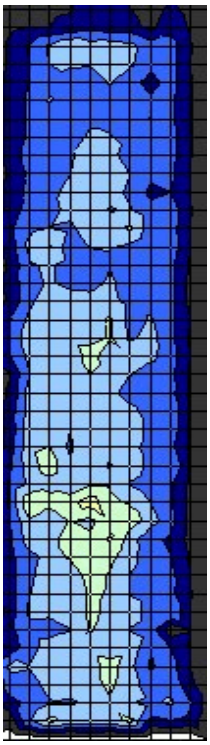

Figure 4.17
Thermal Scan Showing Differential Temperatures Using External Heat

Figure 4.18
Heated Differential Legend (°F)

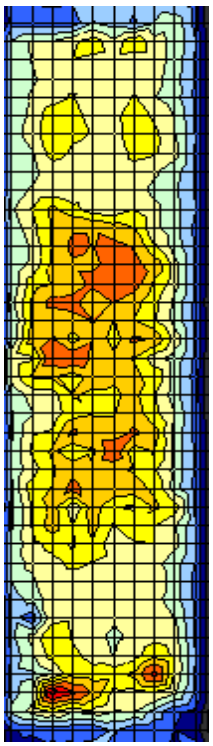

Figure 4.19 Air Logistics Pile Without Epoxy Coating

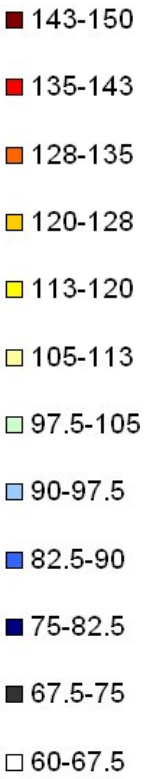

Figure 4.20 Surface Temp (°F)

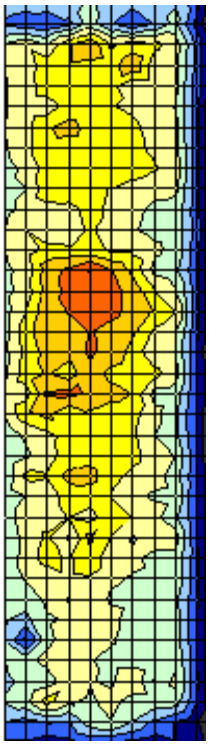

Figure 4.21 Air Logistics Pile With Epoxy Coating

Table 4.1 University of South Florida's DEIT System Properties [15]

Number of Probes	10 x Omega model OS136-1-MV-F
Spectral Range	5 - 14 μm
Weight	80 lbs (including steel frame)
Accuracy	± 4.4 °C or ± 3%
Repeatability	1% of reading
Temperature Range	-18 °C to 204°C
Scanning Frequency	5 Hz
Scanning Speed	1 in/sec
Energy (Heat) Output	42 Joules/in^2
Approx. Cost	$4,000

Table 4.2 FLIR ThermaCAM® P65HS Properties [14]

Thermal Sensitivity at 50/60 Hz	0.05°C at 30°C
Detector Type	Focal Plane Array (FPA) uncooled microbolometer, 320 x 240 pixels
Spectral Range	7.5 - 13 μm
Weight	4.4 lb
Accuracy (% of reading)	± 2°C or ± 2%
Temperature Ranges	-40°C to 120°C or 0°C to 500°C
Scanning Speed	N/A (Instantaneous)
Approx. Cost	$38,000

Chapter 5 Test Results

5.1 Initial Visual Inspection

From a simple visual inspection of the piles, it was immediately seen that those repaired with the pressure system appeared to have the smoothest surface finish. Piles F1 and F2 (Fyfe systems in conjunction with pressure bag), in particular, had a near-flawless surface with only minimal wrinkles. Pile F3 (Fyfe control pile) had the next best appearance followed by pile F4 (Air Logistics system in conjunction with pressure bag).

Both the control and vacuum bagged Air Logistics piles, by contrast, exhibited large wrinkles with deep folds and wrinkles in the FRP fabric as seen in Figure 5.1.

5.2 Acoustic Testing Results

The most obvious result of the acoustic testing was that Fyfe piles utilizing the pressure bag system appeared to have significantly greater areas of satisfactory bond. Zero delamination was detected on Fyfe piles F1 and F2, which correlated well to their visual appearance. Some areas of grade “B” delamination (hollowness detected) were found on Fyfe pile F3, though there was no obvious grade “C” delamination as shown in Figure 5.4. The entirety of the acoustic results are shown in Appendix C.

The Air Logistics piles appeared to have generally larger amounts of delamination than the Fyfe piles. The improvement systems did not appear to have a positive affect, as shown in Figure 5.29. Interestingly, both the vacuum bagged and

pressure bagged Air Logistics pile exhibited greater amounts of possibly delaminated areas than the control pile. Of the remaining Air Logistics piles, A1 had the greatest occurrence of grade “C” delamination. A3 seemed to have the largest grade “B” delamination, mostly concentrated in the bottom half of the FRP area.

The following general trends were noted. First, the suspected hollow areas were typically in the middle of the face, instead of on the pile edges. This is thought to be because as the FRP is stretched tight around the square pile, it fits most snugly around the edges and can become somewhat slack in the center.

In addition, delamination seemed to occur more frequently in a vertical line which followed the position of where the overlap line had been. This overlap line is where the bag attaches to itself, where one fabric layer sits on top of another. The triangle that is formed as a result of this makes it difficult to apply in that vertical area as shown in Figure 5.5. Lastly, areas of delamination appeared most often either at or below the waterline height on the pile.

5.3 Thermographic Analysis Results

In general the thermographic analysis using the DEIT system exhibited a very strong correlation with the results of the acoustic analysis. It appeared that the thermography picked up not only all of the delamination detected by the acoustic test, but it also detected additional areas of delamination and provided a more exact location. As with the acoustic test, delamination was more concentrated in the center of the pile face and not at the edges. After comparison with the pull-off tests (detailed later in the

thesis), any area that exhibited a temperature of 97.5°F or greater was considered delaminated. The entirety of the thermographic results are shown in Appendix C.

5.3.1 Fyfe Piles Thermography

As with the acoustic and visual inspections, the Fyfe piles appeared to have better quality bond than the Air Logistics piles. As shown in Figures 5.6-5.13, Fyfe piles which had been pressure bagged (F1 and F2) looked better than the Fyfe control pile (F3) and demonstrated minimal thermal anomalies. Acoustic testing suggested F1 and F2 to be of equally perfect bond quality.

However, the subsequent DEIT test suggested that both piles exhibited similar bond quality although delamination was detected on both. As stated previously, a temperature of 97.5° F or greater was taken to indicate probably delamination.

True to its acoustic test, the thermal test of F3 showed larger areas than F1 and F2. Unusually, however, Face “B” on pile F3 showed clear delamination with the thermal test where none had been detected acoustically.

5.3.2 Air Logistics Piles Thermography

Piles A1, A3, A4 and F4 (the control pile, two vacuum bagged piles, and pressure bagged pile respectively) all demonstrated large areas of delamination over the majority of their repair areas. Pile A1 appeared to possess somewhat better bond than the other Air Logistics piles. A3's delamination as seen by the DEIT clearly paralleled its acoustic analysis, as they both showed a greater extent of delamination on the bottom half of the pile.

5.4 Pull-off Testing Results

The pull-off testing was supposed to serve as the factual baseline by which the NDT was judged. However, it was more difficult to perform head-to-head comparisons of piles with the pull-off testing. This was in part because of physical deformities on the FRP surfaces and the resulting disparity in available testing areas. The metal testing dolly used in a pull-off test requires a flat, relatively smooth surface on which to adhere. If the surface is irregular then it is possible that only certain portions of the dolly will become attached to the FRP.

As a result, when the dolly is pulled off the surface area used to calculate tensile stress is no longer known. If this situation goes unnoticed then the test will record artificially low bond strength values, owing to the fact that the actual test area is smaller than the theoretical area. Therefore the dollies could only be placed in areas where the FRP surface remained flat and smooth, and these areas were not consistent among the different piles.

Surface irregularities can also artificially reduce the bond strength reading because of subsequent eccentricity in the testing device. If one of the three legs of the pull-off device is higher than the others, the device will be applying pull-off force at an angle other than 90°F from the pile face. An overturning moment (lever arm) is then developed in addition to the tensile force. This moment cannot be accounted for by the pull-off device but still reduces the apparent capacity of the specimen.

An overturning moment may also affect the test's mode of failure. What might have been a full concrete failure becomes a partial failure as one side of the dolly lifts up.

Instead of a pure tensile failure the dolly is in effect unzipped along its base by shear forces [13].

Pull-off tests were evaluated mainly on the basis of pull-off strength. Modes of failure in different areas did not seem to be consistent, which may be in part due to the reasons mentioned previously. Satisfactory bond strength was taken as equal to or greater than 200 psi per ACI standards [8].

5.4.1 Fyfe Piles Pull-offs

Pull-off tests on the Fyfe piles consistently yielded higher bond strengths then on the Air Logistics piles. They also exhibited a greater percentage of satisfactory bond strengths (>200 psi) as shown in Figure 5.32. Average bond strengths were consistently greater above the waterline than below the waterline for any given Fyfe pile. There was also a greater percentage of satisfactory pull-offs above the waterline than below.

The addition of the pressure bag to the Fyfe piles typically produced an improvement of 5-10% in both percentage of satisfactory tests and average bond strength as shown in Figures 5.34 and 5.35. There was also typically a larger improvement below the waterline than above, possibly because there was more room for improvement below the waterline.

5.4.2 Air Logistics Piles Pull-offs

Bond strengths were weaker overall for Air Logistics piles than for Fyfe piles, and there was a smaller percentage of satisfactory bond tests. Regions below the

waterline on the control and vacuum bagged piles, in particular, typically demonstrated zero bond strength.

It was often impossible to perform a pull-off test in these areas because the testing area was so weak that it would break off as it was being cored. In these cases, half of the failed-test locations were automatically assumed delaminated. The other half were not counted.

The vacuum bagged piles showed little to no improvement over the control pile. The pressure bagged pile, however, dramatically increased both average bond strengths and percentage of satisfactory adhesion tests as shown in Figures 5.34 and 5.35. The pressure bag consistently improved bond both above and below the waterline.

5.5 Parametric Study of Bond Strength Cut-off

A minimum acceptable bond strength of 200 psi was used for this research, which corresponds to ACI 440 [8] specifications for bond-critical FRP applications like strengthening columns for flexure. For contact-critical applications like column confinement, however, no minimum bond strength is specified. For this reason a parametric study was performed to determine how results would differ if a minimum acceptable bond strength of 100 psi were used instead.

As shown in Figures 5.31 and 5.33, the reduction in acceptable adhesion strength made the bond improvement for Fyfe piles significantly greater below the waterline than above. When 200 psi had been used originally the improvements had been relatively equal. There was no noticeable change in the Air Logistics vacuum bagged piles.

However, the Air Logistics pressure bagged piles switched their most improved area from above the waterline to below the waterline.

As expected, the Fyfe piles became nearly perfect when examining the percentage of satisfactory tests after the acceptable adhesion strength was lowered. The Air Logistics pressure bag results closely resembled the Fyfe piles as well. The Air Logistics control and vacuum bagged piles remained inferior to the other piles, and still had relatively poor acceptance rates below the waterline.

5.6 Comparison of NDT and Pull-off Testing Results

In general both acoustic and IRT testing suggested relatively small amounts of delamination on the Fyfe piles, with pile F3 (control pile) having more delaminated area than either of the 2 pressure bagged piles. It also indicated that the Air Logistics piles were delaminated to a much greater extent than the Fyfe piles. All the Air Logistics piles appeared similar in that they all showed probable delamination over the majority of their faces.

Pull-off testing confirmed that pile F3 possessed lower bond strengths and fewer areas of acceptable adhesion testing than the pressure bagged Fyfe piles. However, the 5-10% improvement produced by the pressure bag was not as dramatic an improvement as the thermal testing suggested. Pull-offs also confirmed the NDT's suggestion that Fyfe piles exhibited superior bond strength and fewer areas of unsatisfactory bond when compared to Air Logistics piles.

NDT correctly judged the Air Logistics piles as generally inferior to the Fyfe piles, however it was imprecise in distinguishing between degrees of delamination within Air Logistics piles. Air Logistics pile F4 (pressure bagged), which appeared similar to the other Air Logistics piles to NDT, turned out to possess significantly better bond characteristics than its peers. This included a 344% improvement in average bond strength below the waterline as shown in Figure 5.35.

5.6.1 Difficulties With NDT

It is possible that the NDT's precision was compromised by certain Air Logistics-specific issues, namely the non-structural veil and the lesser degree of fiber saturation which are discussed more in the next chapter. As seen in Figure 5.36, Fyfe piles generally provided better agreement between NDT and pull-off testing whereas there was more disparity in the Air Logistics piles. Comparison of the percentage of satisfactory area or tests between the acoustic and pull-off testing, respectively, yields interesting results. The pull-off testing shows all Fyfe piles to have greater percentages of satisfactory tests with the pressure bagged Air Logistics lagging slightly behind. The control and vacuum bagged Air Logistics piles, by comparison, are abysmal.

When acoustic testing is used on these same piles, however, the Air Logistics piles which are (in reality) badly delaminated falsely appear to have bond qualities similar to that of the Fyfe piles. The three types of piles that are decent in actuality (Fyfe control and pressure bagged, Air Logistics pressure bagged) appear relatively unchanged from the pull-off test results. There are 2 possible reasons for this occurrence.

First, it is thought that acoustic testing will miss at least 20-30% of delaminated areas [9]. Therefore if piles have superior bond quality then there will not be as many delaminated areas which are able to be missed: the acoustic testing will therefore be more accurate. A pile which is 100% satisfactory leaves no room for error in acoustic analysis. Increasing the amount of delaminated areas, however, increases the amount of areas which acoustic testing is able to inaccurately portray. Therefore it makes sense that acoustic testing was more accurate on superior piles than it was on inferior piles.

The second possible reason for this disparity is that of accidental relative comparison. When testing Fyfe piles, the baseline "A" reading (which made up the majority of the pile) was likely to have been an area of greater than 200 psi adhesion strength. Therefore any areas which sounded differently were marked up as delaminated areas. On the Air Logistics piles, however, it is likely that the majority of the pile was sub-200 psi. The baseline reading was probably a delaminated area to start with. Any areas which sounded different were marked as delaminated when in reality the majority of the pile was delaminated. Therefore areas which sounded relatively worse were marked as delaminated and areas which sounded relatively better were marked as sound. But it is probable that if the Air Logistics' supposedly "good" areas could have been compared to the Fyfe's actually "bad" areas, it would have been seen that both areas were in fact delaminated.

Interestingly, the initial visual inspection noted that Fyfe piles F1 and F2 had the smoothest surface finishes, followed closely by Fyfe pile F3 and then Air Logistics Pile F4. The control and vacuum bagged piles were noted to have the worst physical

appearances, being laden with deep folds and wrinkles. Therefore when considering *relative* adhesion properties between different piles, the initial visual inspection was very accurate.

5.6.2 Fyfe Piles NDT

Fyfe pull-off values, shown partially in Figures 5.15-5.17, generally corresponded well to the non-destructive testing. The lowest values are seen to be in the center of the face and in the lower half of the pile which corresponds to the NDT. F3 face A and F1 face B both appear to possess better bond above the waterline which is also in concurrence. Similarly, F3 face C agrees with the DEIT system by showing 75% good both above and below the waterline. F2 C and F1 C both appear slightly better below the waterline than above, which also corresponds to the NDT.

Pull-offs on F1 D show the bottom to be significantly worse than the top, which is dissimilar from the DEIT test.

It is not surprising that some areas of Fyfe piles which did not appear to have delamination were, in fact, delaminated. It is common practice in concrete slab corrosion surveying to use metal chains to detect delaminated areas and to multiply the area of delamination found x 100%, to estimate the delaminated area that will be found when the concrete gets removed [7].

This is partly because the corrosion-delaminated areas are surrounded by areas which are on the verge of delaminating, and when the concrete is chipped out and replaced the concrete which is already weakened will break off as well. But the

multiplication factor is also used because, for whatever reason, examining the outside of an object can't always reveal exactly what is on the inside.

5.6.3 Air Logistics Piles NDT

NDT indicated that Air Logistics piles were generally delaminated, and in that regard it was precise as shown in Figures 5.18-5.21. However, the NDT was not as successful in determining which regions of piles were more delaminated and which piles were more delaminated than others. Both acoustic and thermal testing on pile A3 indicated a greater extent of delamination below the waterline than above. This was confirmed by the pull-off tests, as the below-waterline testing areas were so weak that could not undergo coring.

Pile A1 face C, however, displayed similar pull-off results below the waterline although NDT had indicated otherwise. Correlations between NDT and pull-off testing were stronger on face D of that same pile. In this case the NDT had correctly anticipated lower bond strengths below the waterline.

On pile F4, NDT again indicated that bond strengths were generally diminished below the waterline and this proved to be correct. However, as previously mentioned the pile's thermal scan provided no clue that it possessed higher bond strengths and fewer areas of unsatisfactory bond.

Figure 5.1 Wrinkles on Air Logistics Piles

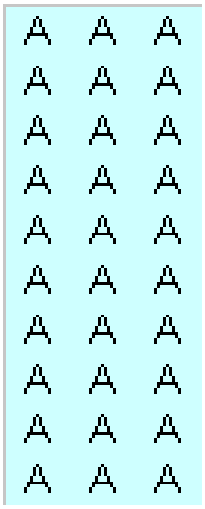

Figure 5.2 Typical Pile F1 (Fyfe Pressure Bag)

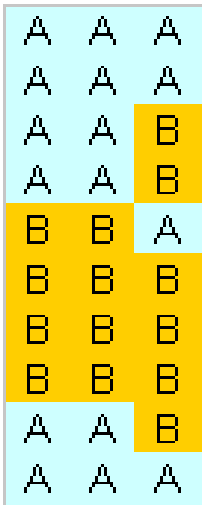

Figure 5.3 Typical Pile F4 (Air Logistics Pressure Bag)

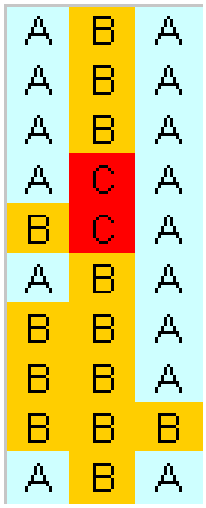

Figure 5.4 Typical Pile A1 (Air Logistics Control)

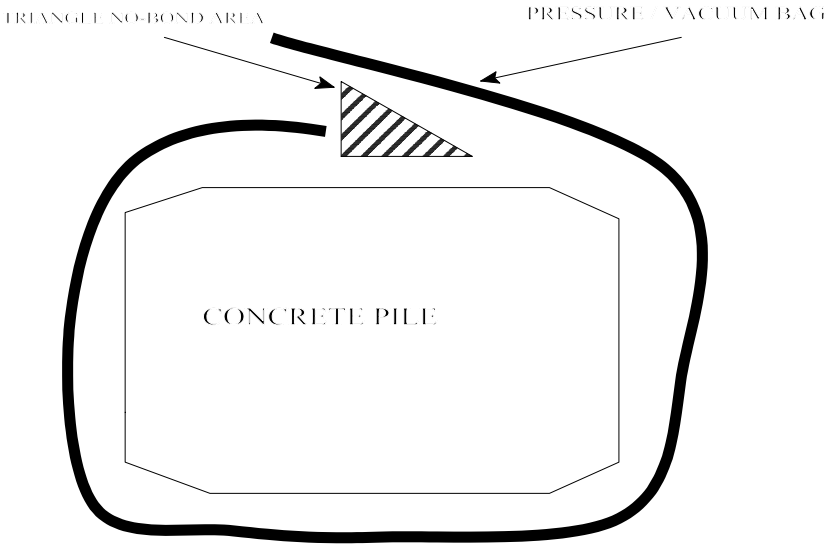

Figure 5.5 No-bond Area Caused by Triangular Overlap Region

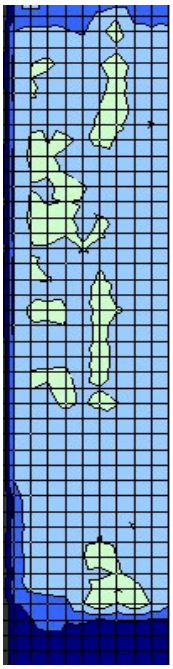

Figure 5.6 Typical Pile F1 Thermal Scan

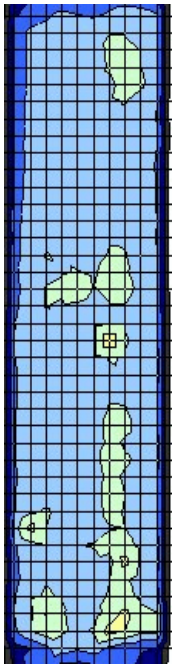

Figure 5.7 Typical Pile F2 Thermal Scan

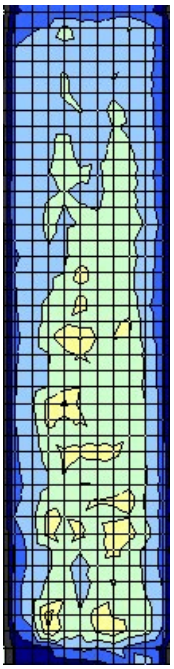

Figure 5.8 Typical Pile F3 Thermal Scan

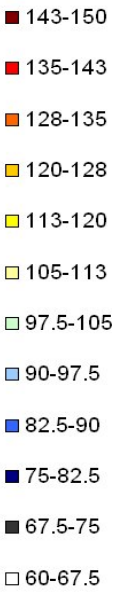

Figure 5.9 Fyfe Piles Thermal Legend (°F)

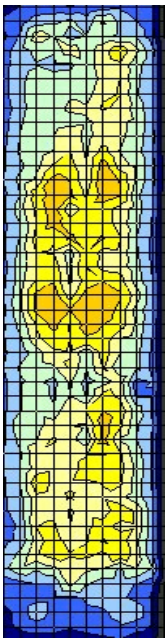

Figure 5.10 Typical Pile A1 Thermal Scan

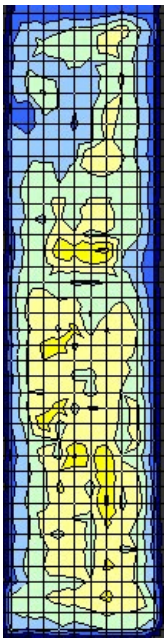

Figure 5.11 Typical Pile A3 Thermal Scan

Figure 5.12 Typical Pile A4 Thermal Scan

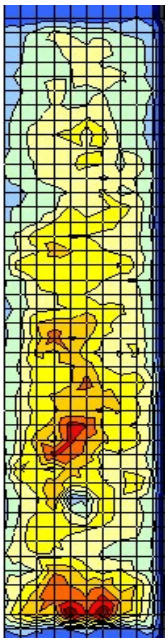

Figure 5.13 Typical Pile F4 Thermal Scan

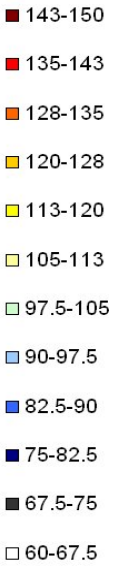

Figure 5.14 Air Logistics Thermal Legend (°F)

x	19	197
77	19	236
x	x	162
38	x	306
x	x	x
0	x	0
x	0	x
0	x	77
x	0	x
0	x	0

Figure 5.15
Typical Pile A1
Pull-off Values
(psi)

x	x	x
124	116	108
209	85	128
50	89	81
58	54	124
x	0	x
0	x	0
x	0	x
0	x	0
x	0	x

Figure 5.16
Typical Pile A3
Pull-off Values
(psi)

x	x	x
252	85	368
124	58	x
x	x	x
85	x	116
x	65	100
85	54	89
77	x	77
108	58	x
x	x	x

Figure 5.17
Typical Pile A4
Pull-off Values
(psi)

x	x	x
186	352	263
232	252	217
259	162	224
124	x	236
135	x	201
356	93	182
244	x	62
232	108	116
155	155	155

Figure 5.18
Typical Pile F4
Pull-off Values
(psi)

x	x	x
384	124	228
271	147	x
352	263	x
306	x	333
182	x	x
x	248	x
387	201	x
x	x	201
x	x	x

Figure 5.19
Typical Pile F1
Pull-off Values
(psi)

x	x	x
306	228	x
x	x	x
x	310	x
x	318	x
x	155	x
x	256	x
x	x	x
x	162	294
x	x	x

Figure 5.20
Typical Pile F2
Pull-off Values
(psi)

x	x	x
279	x	298
228	387	341
298	252	384
387	116	267
x	x	333
186	x	151
x	x	248
356	124	x
x	x	x

Figure 5.21
Typical Pile F3
Pull-off Values
(psi)

x	VEIL	FRP
PC	VEIL	EPX
x	x	PC
FRP	x	PC
x	x	x
x	x	x
x	x	x
x	x	FRP
x	x	x
x	x	x

Figure 5.22
Typical Pile A1
Pull-off Failure
Modes

x	x	x
FRP	PC	FC
FRP	VEIL	PC
FRP	FRP	FRP
VEIL	FRP	FRP
x	x	x
x	x	x
x	x	x
x	x	x
x	x	x

Figure 5.23
Typical Pile A3
Pull-off Failure
Modes

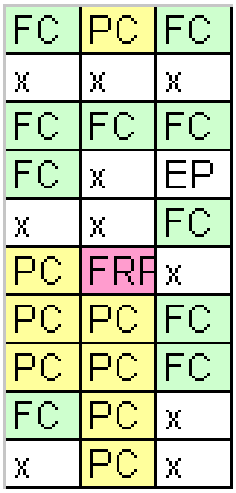

Figure 5.24
Typical Pile F1
Pull-off Failure
Modes

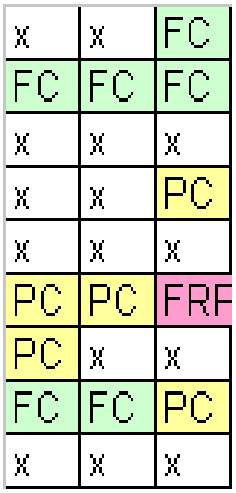

Figure 5.25
Typical Pile F2
Pull-off Failure
Modes

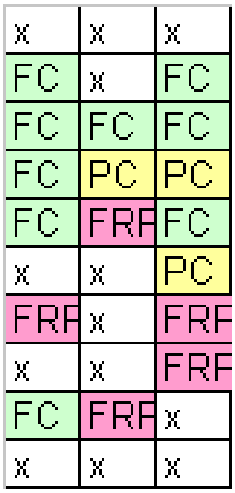

Figure 5.26
Typical Pile F3
Pull-off Failure
Modes

Figure 5.27
Typical Pile A4
Pull-off Failure
Modes

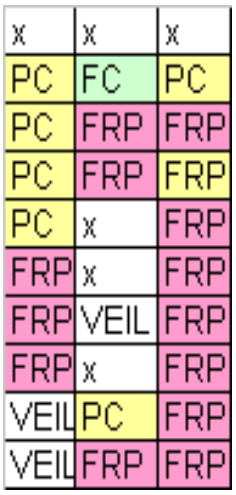

Figure 5.28
Typical Pile F4
Pull-off Failure
Modes

Appendix C shows the graphic results in their entirety including visual, acoustic and thermal test methods for every pile and face.

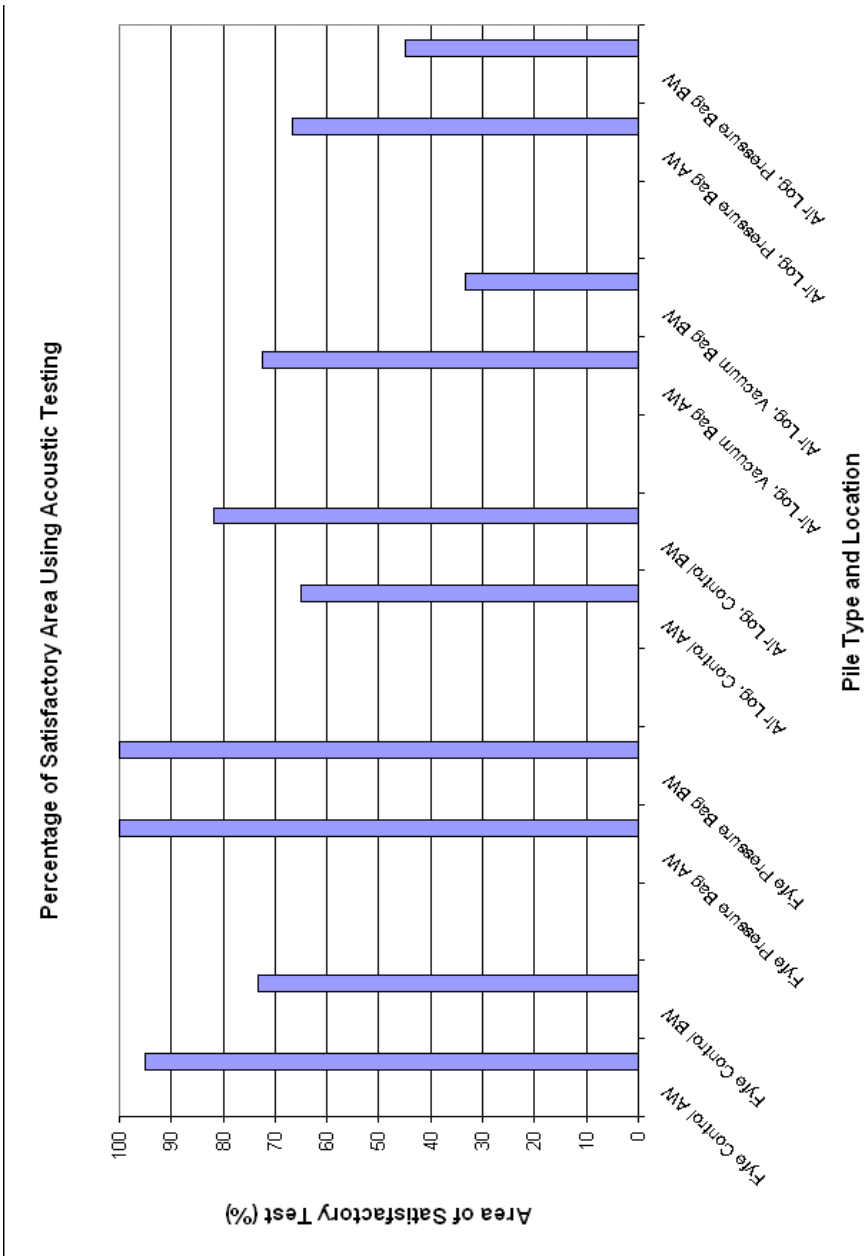

Figure 5.29 Satisfactory Tests Using Acoustic Method

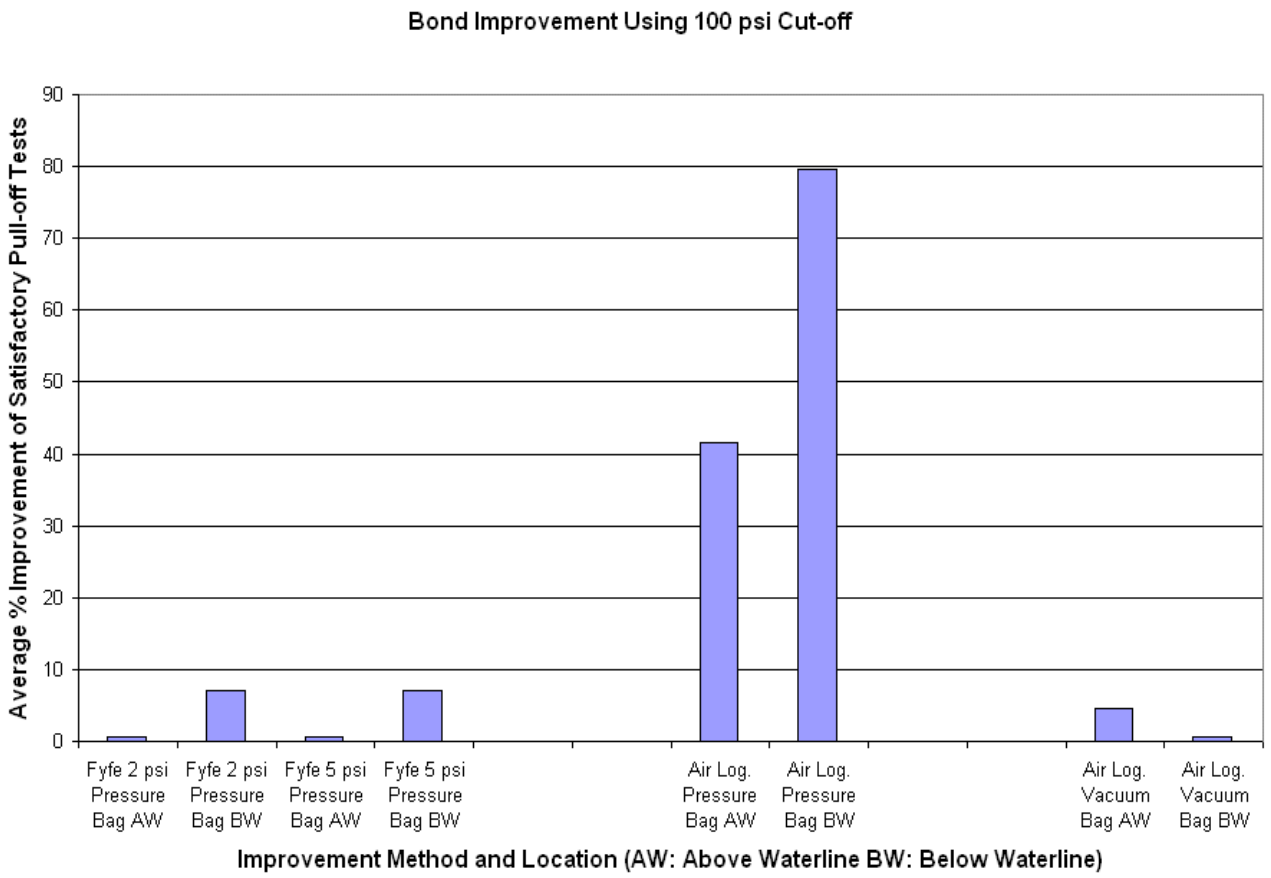

Figure 5.30 Bond Improvement Using 100 psi Cut-off

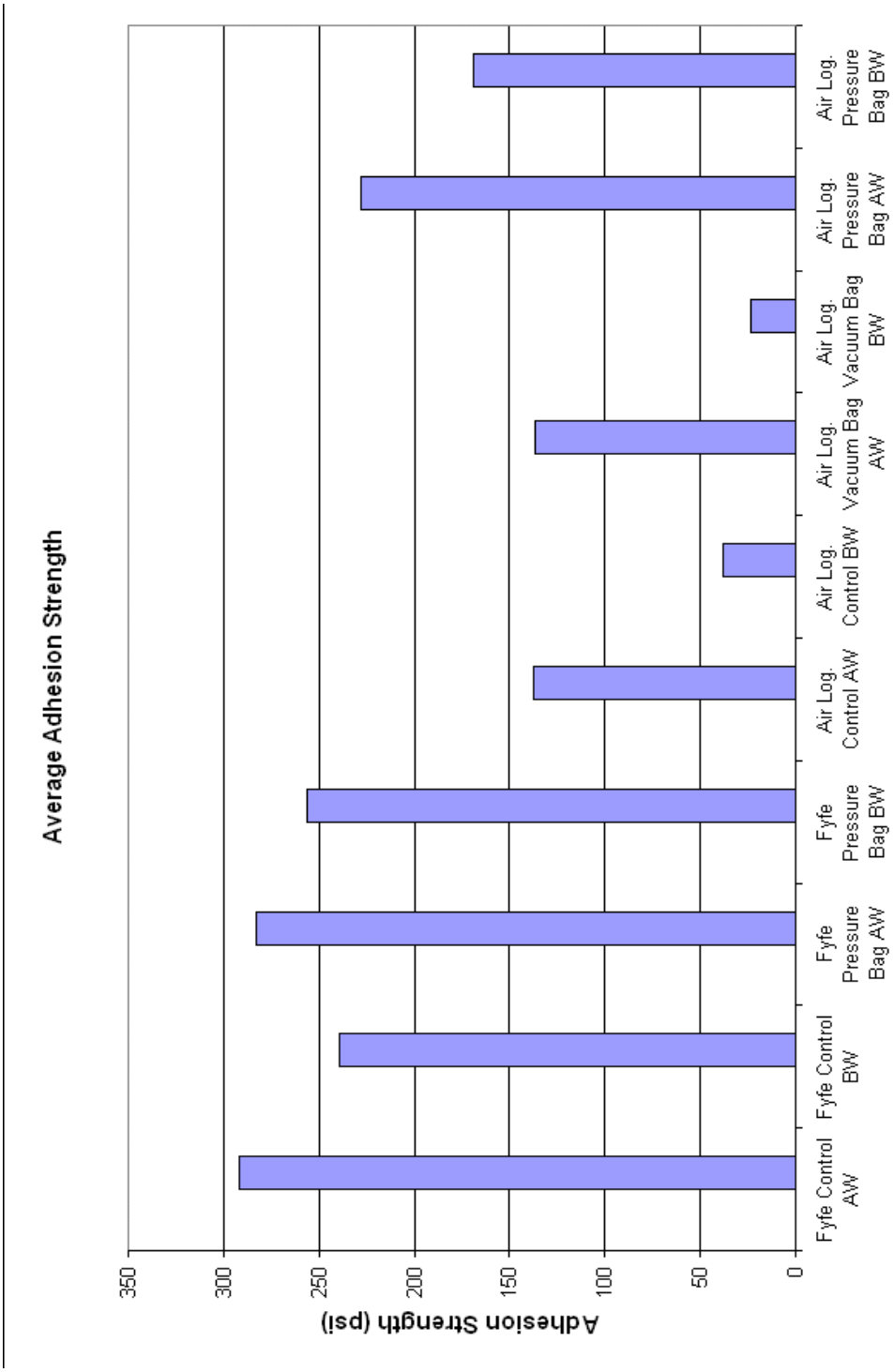

Figure 5.31 Average Adhesion Strengths

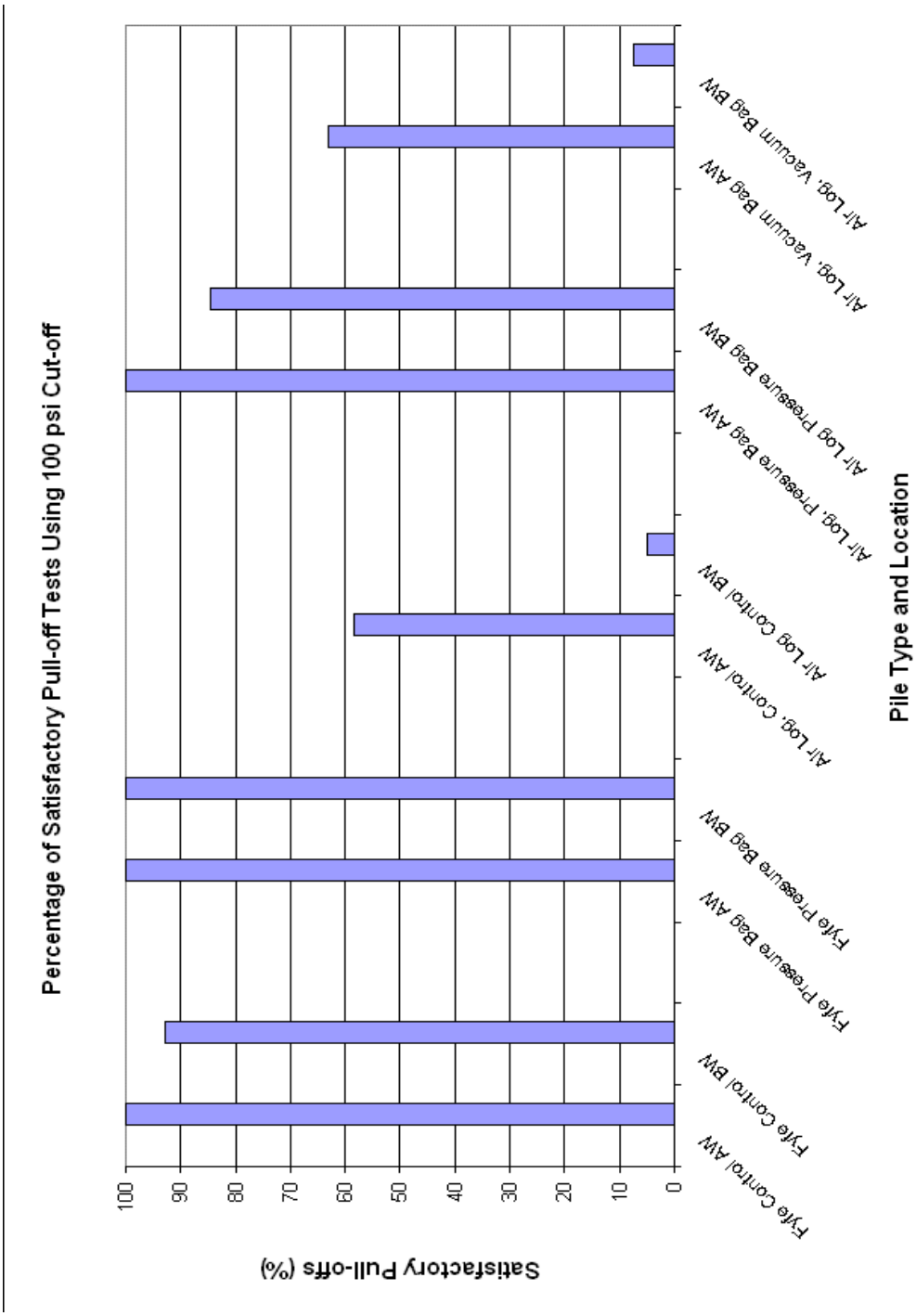

Figure 5.32 Satisfactory Pull-offs Using 100 psi Cut-off

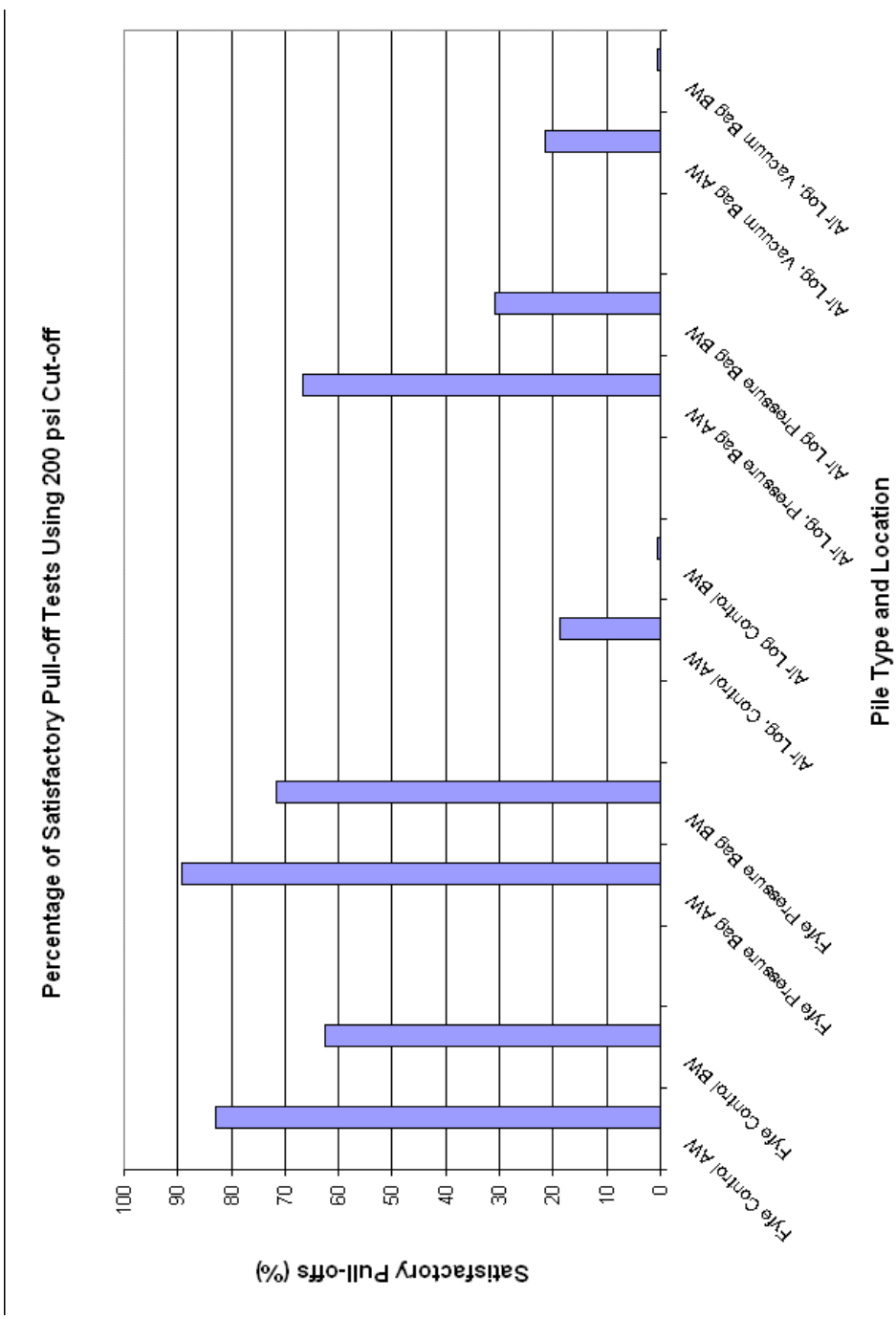

Figure 5.33 Satisfactory Pull-offs Using 200 psi Cut-off

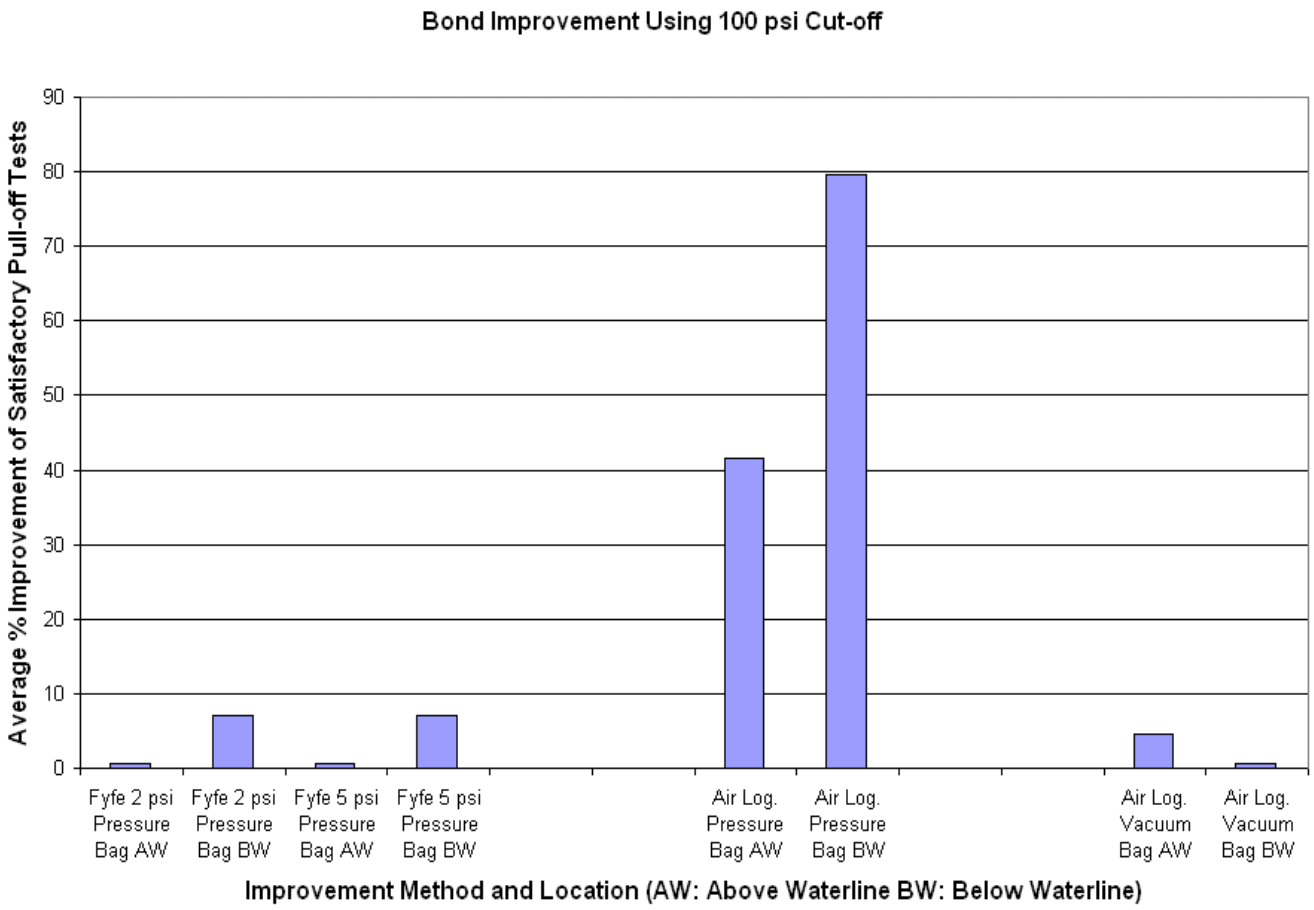

Figure 5.34 Bond Improvement Using 100 psi Cut-off

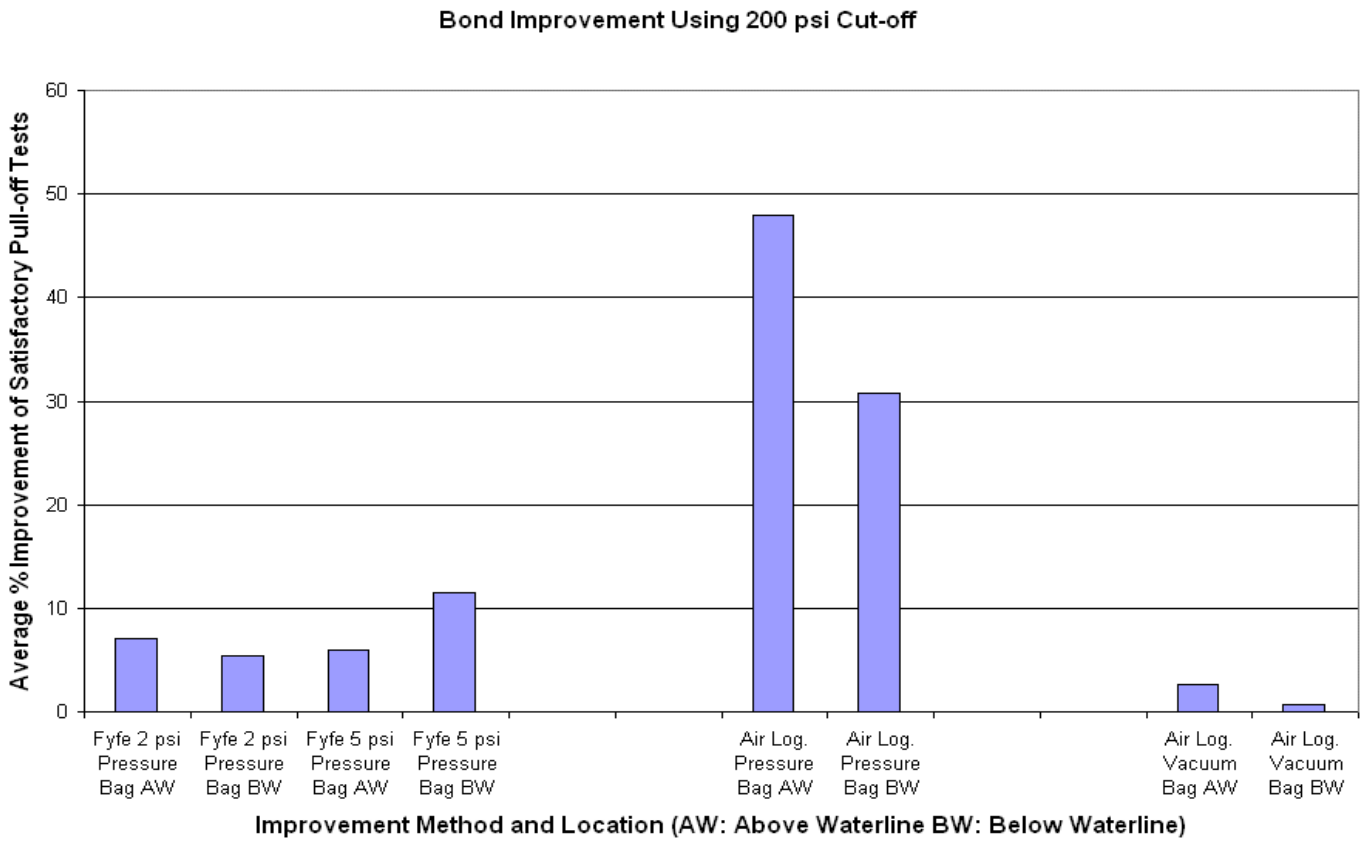

Figure 5.35 Bond Improvement Using 200 psi Cut-off

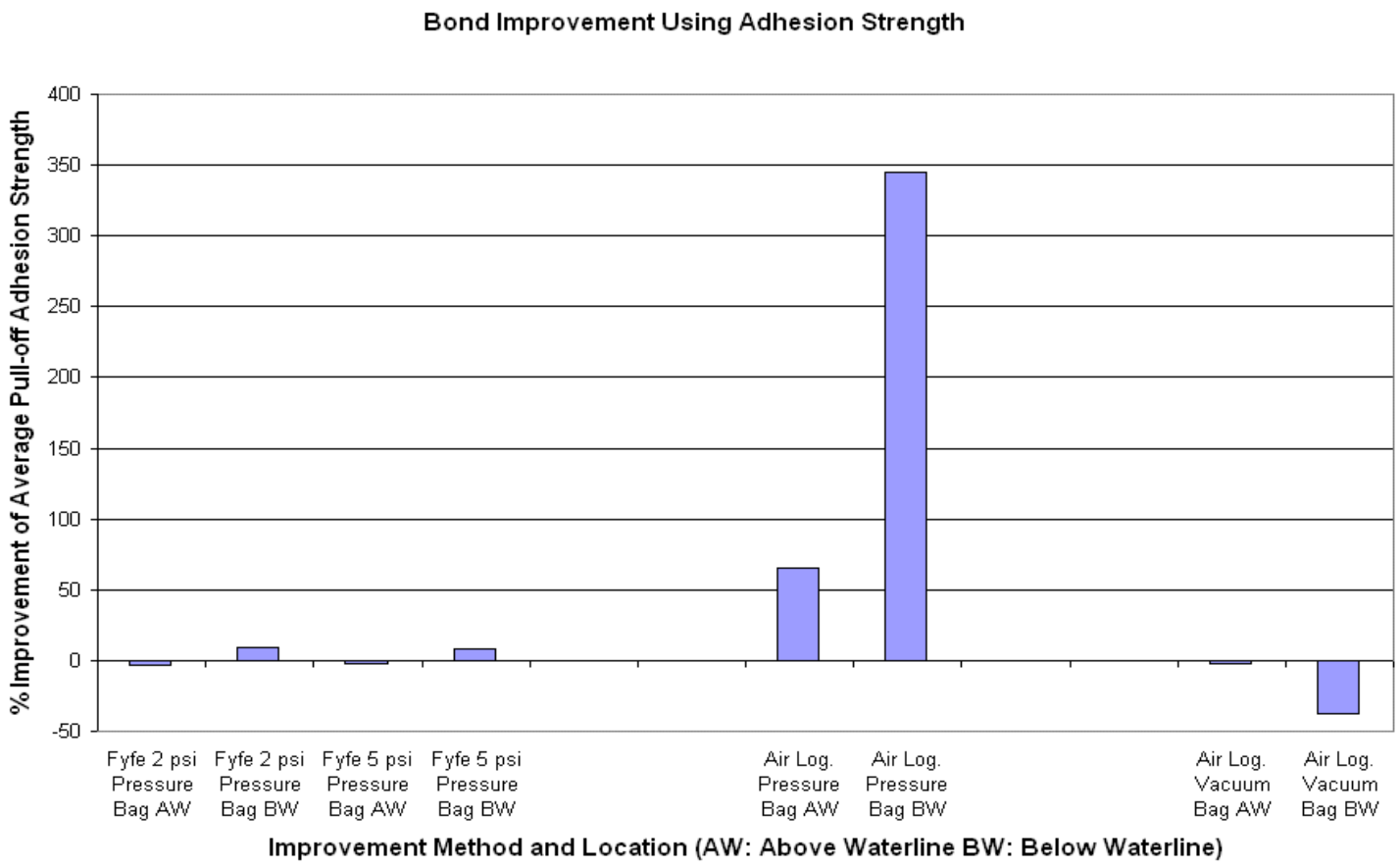

Figure 5.36 Bond Improvement Using Raw Adhesion Strengths

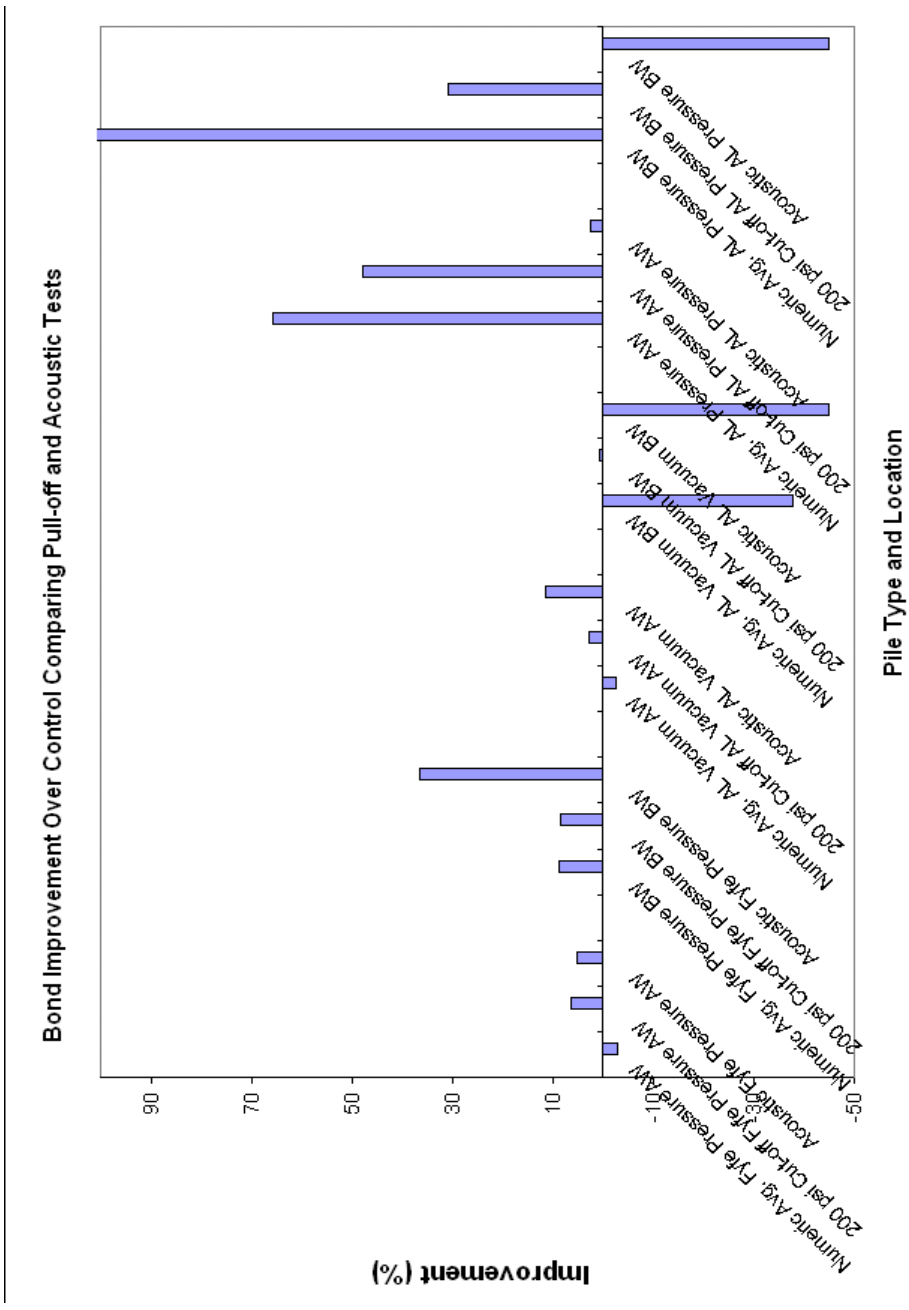

Figure 5.37 Comparison of Bond Improvement by Acoustic and Pull-off Methods

Chapter 6 Conclusion and Summary

6.1 Conclusions

The research in this thesis has shown that pressure bagging can be used as an effective method to improve FRP bond to concrete piles in areas both above and below the waterline. Vacuum bagging is not likely to be as effective because of the inherent difficulties involved in obtaining an airtight seal on a porous material like concrete.

All areas of the pile gained higher bond strengths through pressure bagging. However, areas which were the most difficult to achieve good bond before–particularly below the waterline and in the center of the pile face–remain the most likely areas to demonstrate bond strength deficiencies.

Acoustic analysis, thermographic analysis and pull-off tests all demonstrated similar results when examining the bond strength on Fyfe piles. Thermographic analysis using the DEIT system, in particular, seems to be promising as it can easily scan the entire pile face and provide easily interpreted results. It is less subjective than acoustic analysis. It yields results faster than pull-off testing, is non destructive, and is not limited by surface profile deformities as is pull-off testing.

Acoustic and thermographic testing were not in agreement with the pull-off tests regarding the Air Logistics piles, however. As mentioned previously, it is possible that the Air Logistics FRP's external veil, when separated from its structural layer, provides the same heat and sound energy response as when the FRP is debonded from the

substrate. This veil is the outermost layer of the FRP fabric, which helps to protect the structural fibers beneath but has no strength capacity itself.

It is also possible for the amount of resin saturation in the fibers to affect the FRP's thermal and acoustic signature. It was noticed that there was a greater amount of apparently dry, exposed fibers in the Air Logistics FRP than in the Fyfe FRP. Any small voids between the fibers, if not filled with resin, would instead be filled with air.

These air voids would be able to transfer neither heat nor sound energy as effectively as resin-filled pockets. They would also give acoustic and thermal testing the appearance of unbonded areas. The presence of these air voids would not necessarily reduce the FRP adhesion strength. As a result, FRP in this situation may actually have a stronger bond than nondestructive tests indicate, as was the case with Air Logistics pile F4.

6.2 Recommendations for Future Research

It is not known whether saltwater has a different effect than freshwater on the FRP polymerization reaction. It is also possible that the different types of glass used in the fibers may react differently to saltwater, or possess different emissivity/reflectivity values which would affect the infrared testing. These ideas should be investigated further.

It would be preferable to install a laser rangefinder on the DEIT system, so that a consistent distance from the pile could be achieved every time. In this research the distance was approximated using plastic "whiskers" mounted to the thermal probe box.

It would also be beneficial to manufacture a mechanical addition to the pull-off device. This would ideally allow the pull-off device to apply tensile force only in a direction perpendicular to the orientation of the fibers. This could be as simple as a leg extension system which allows the individual legs of the device to be lengthened or shortened depending on the physical deformation of the testing area. Regardless of the means, the result would be that bond strength values and failure modes would more precisely represent the existing material interface and not be compromised by eccentric loadings.

Lastly, the triangle problem caused by the wrap line should be eliminated. The wrap line, although only on one of the four faces at any given time, appears to cause increased delamination in a vertical pattern down the pile.

References

[1] Emmons, Peter. *Concrete Repair and Maintenance Illustrated*. RS Means. 1993.

[2] "Florida Quick Facts", The State of Florida.com Website. Website. <http://www.stateofflorida.com/Portal/DesktopDefault.aspx?tabid=95> Last Accessed on Feb 3 2007.

[3] "Zinc-Mesh Jacket System Improves Corrosion Control", Better Roads Magazine Website. Website. <http://obr.gcnpublishing.com/articles/nov02f.htm>Last Accessed on Feb 3 2007.

[4] Fyfe Co. LLC. Tyfo SW epoxy, San Diego, CA.

[5] AQUAWRAP 22-77 Resin system, Air Logistics, Pasadena, CA.

[6] Thin Film Technology Inc., Houston TX.

[7] Personal interview. Bud Karins, CEO, Karins Engineering Group Inc., Feb 20 2007.

[8] ACI 440.2R-02 (2002) *Guide for the Design and Construction of Externally Bonded FRP Systems for Strengthening Concrete Structures,* American Concrete Institute, Farmington Hills, MI.

[9] CFRP Repair of Impact Damaged Bridge Girders, Volume II - Inspection of FRP Composite Repairs Using Infrared Thermography, FDOT Structures Research Report No. 879, January 2005.

[10] Dutta, Shasanka (2006). "Nondestructive Evaluation of FRP Wrapped Concrete Cylinders Using Infrared Thermography and Ground Penetrating Radar." Masters Thesis, Department of Civil and Environmental Engineering, West Virginia University, Morgantown, West Virginia.

[11] Levar, J.L. and Hamilton III, H.R.(2003). "Nondestructive Evaluation of Carbon Fiber-Reinforced Polymer-Concrete Bond Using Infrared Thermography," ACI Materials Journal, Jan/Feb 2003, v. 100, no. 1, pp. 63-72.

[12] Bonaldo et. al (2004). Bond Characterization Between Concrete Base and Repairing SFRC by Pull-off Tests. University of Minho, Azurem, Guimaraes (Portugal).

[13] Personal interview. Dr. Gray Mullins, University of South Florida Associate Professsor, February 26 2007.

[14] FLIR Systems Inc., Wilsonville, OR.

[15] Omega Engineering Inc., Stamford, CT.

[16] “Carbon Fiber-Reinforced Polymer Shows Promise for Repairing Structures”, Georgia Tech Research News Website. Website. <http://gtresearchnews.gatech.edu/newsrelease/BRIDGE.html> Last Accessed on March 10 2007.

Appendices

Appendix A Pull-off Test Results Photographs

This appendix shows the results of pull-off tests taken on the FRP repaired surfaces. The notation is as follows: Pile, Face, Column (1-3) Row (1-10).

Figure A.1 F1 B Col 1 Row 1

Figure A.2 F1 B Col 1 Row 3

Figure A.3 F1 B Col 1 Row 4

Figure A.4 F1 B Col 1 Row 6

Figure A.5 F1 B Col 1 Row 7

Figure A.6 F1 B Col 1 Row 8

Appendix A (Continued)

Figure A.7 F1 B Col 1 Row 9

Figure A.8 F1 B Col 2 Row 1

Figure A.9 F1 B Col 2 Row 3

Figure A.10 F1 B Col 2 Row 6

Figure A.11 F1 B Col 2 Row 7

Figure A.12 F1 B Col 2 Row 8

Figure A.13 F1 B Col 2 Row 9

Figure A.14 F1 B Col 2 Row 10

Appendix A (Continued)

Figure A.15 F1 B Col 3 Row 1

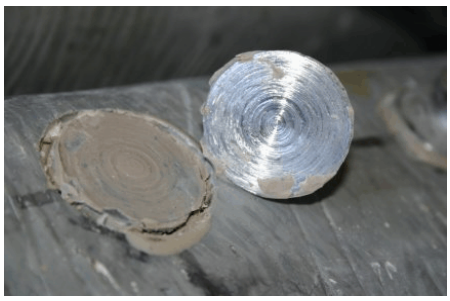

Figure A.16 F1 B Col 3 Row 4

Figure A.17 F1 B Col 3 Row 5

Figure A.18 F1 B Col 3 Row 7

Figure A.19 F1 B Col 3 Row 8

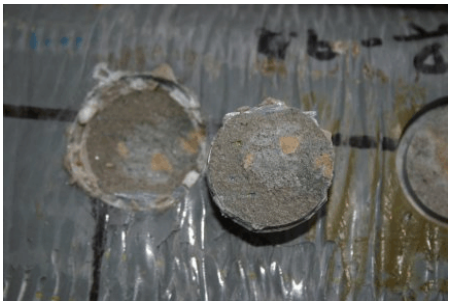

Figure A.20 F1 C Col 1 Row 3

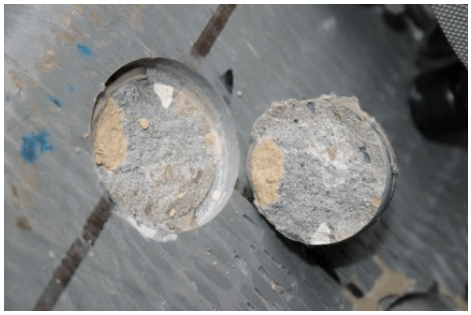

Figure A.21 F1 C Col 1 Row 4

Figure A.22 F1 C Col 1 Row 5

Appendix A (Continued)

Figure A.23 F1 C Col 1 Row 6

Figure A.24 F1 C Col 1 Row 8

Figure A.25 F1 C Col 2 Row 3

Figure A.26 F1 C Col 2 Row 4

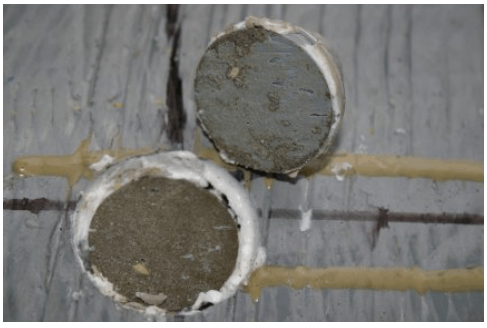

Figure A.27 F1 C Col 2 Row 8

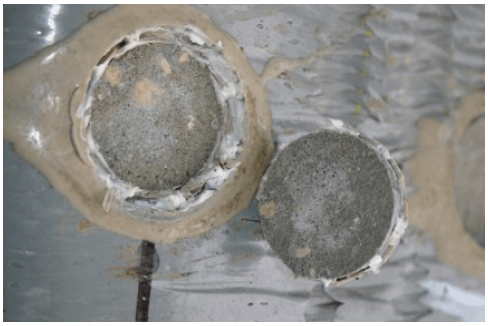

Figure A.28 F1 C Col 3 Row 2

Figure A.29 F1 C Col 3 Row 4

Figure A.30 F1 C Col 3 Row 5

Appendix A (Continued)

Figure A.31 F1 C Col 3 Row 9

Figure A.32 F1 D Col 1 Row 3

Figure A.33 F1 D Col 1 Row 4

Figure A.34 F1 D Col 1 Row 5

Figure A.35 F1 D Col 1 Row 6

Figure A.36 F1 D Col 1 Row 8

Figure A.37 F1 D Col 1 Row 9

Figure A.38 F1 D Col 2 Row 4

Appendix A (Continued)

Figure A.39 F1 D Col 2 Row 5

Figure A.40 F1 D Col 2 Row 6

Figure A.41 F1 D Col 2 Row 7

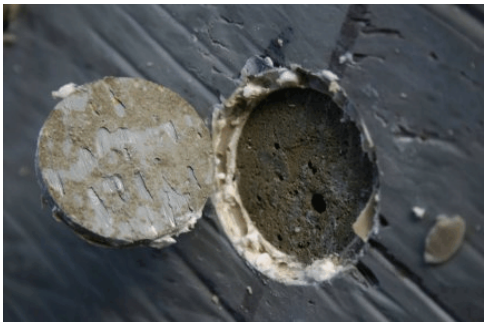

Figure A.42 F1 D Col 2 Row 8

Figure A.43 F1 D Col 2 Row 9

Figure A.44 F1 D Col 3 Row 2

Figure A.45 F1 D Col 3 Row 4

Figure A.46 F1 D Col 3 Row 5

Appendix A (Continued)

Figure A.47 F1 D Col 3 Row 6

Figure A.48 F1 D Col 3 Row 7

Figure A.49 F1 D Col 3 Row 8

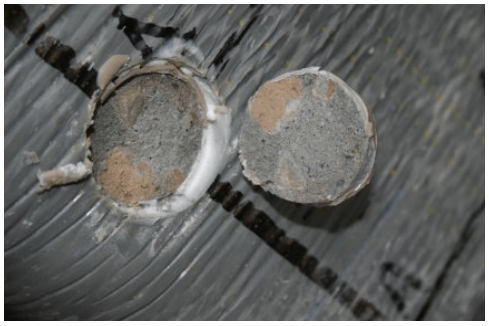

Figure A.50 F2 C Col 1 Row 3

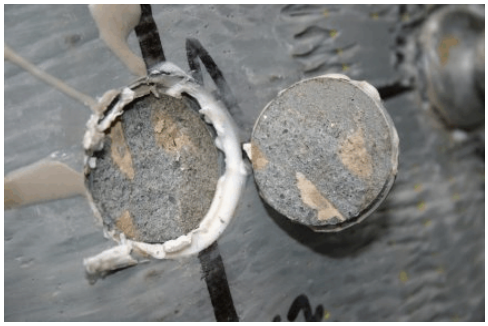

Figure A.51 F2 C Col 1 Row 7

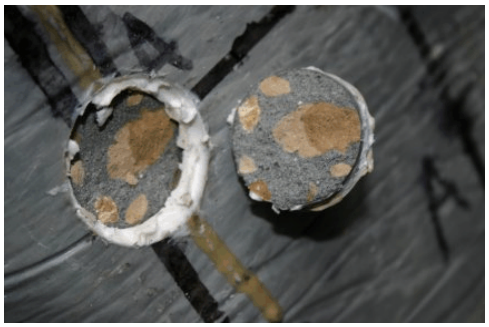

Figure A.52 F2 C Col 1 Row 9

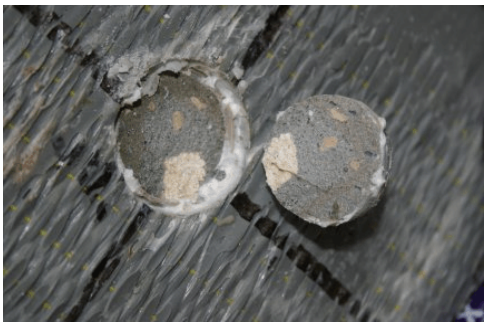

Figure A.53 F2 C Col 2 Row 3

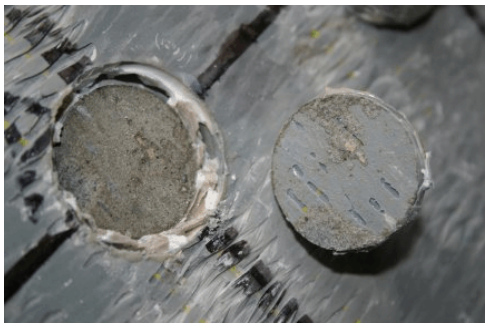

Figure A.54 F2 C Col 2 Row 7

Appendix A (Continued)

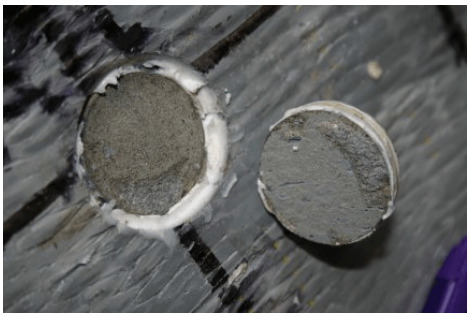

Figure A.55 F2 C Col 2 Row 9

Figure A.56 F2 C Col 3 Row 3

Figure A.57 F2 C Col 3 Row 5

Figure A.58 F2 C Col 3 Row 7

Figure A.59 F2 C Col 3 Row 9

Figure A.60 F2 D Col 1 Row 2

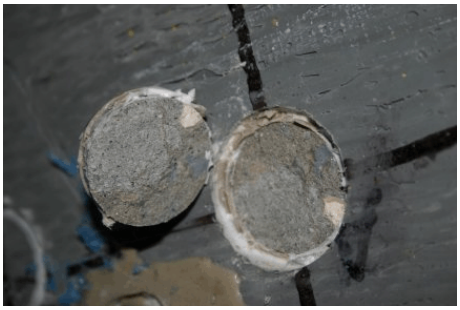

Figure A.61 F2 D Col 2 Row 2

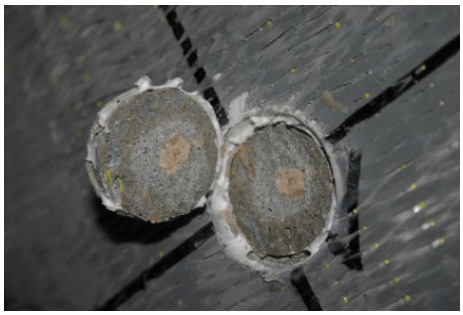

Figure A.62 F2 D Col 2 Row 4

Appendix A (Continued)

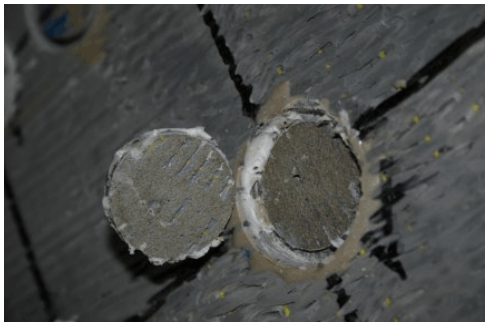

Figure A.63 F2 D Col 2 Row 5

Figure A.64 F2 D Col 2 Row 6

Figure A.65 F2 D Col 2 Row 7

Figure A.66 F2 D Col 2 Row 9

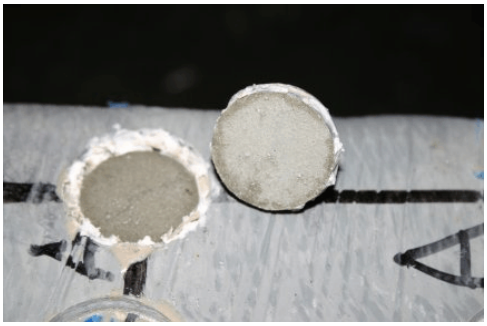

Figure A.67 F2 D Col 3 Row 9

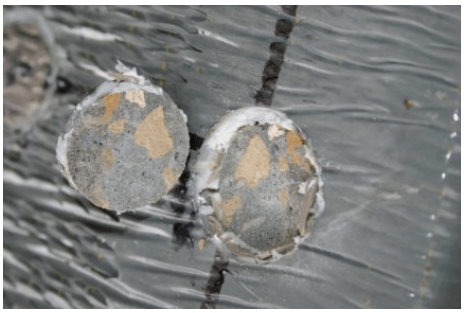

Figure A.68 F3 A Col 1 Row 2

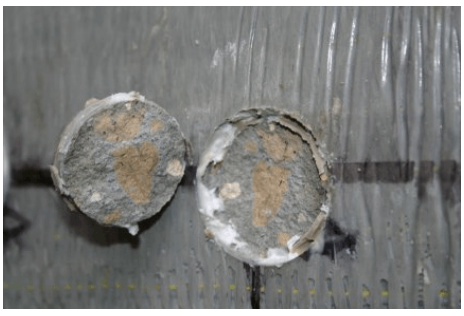

Figure A.69 F3 A Col 1 Row 3

Figure A.70 F3 A Col 2 Row 9

Appendix A (Continued)

Figure A.71 F3 A Col 1 Row 4

Figure A.72 F3 A Col 1 Row 5

Figure A.73 F3 A Col 1 Row 7

Figure A.74 F3 A Col 1 Row 9

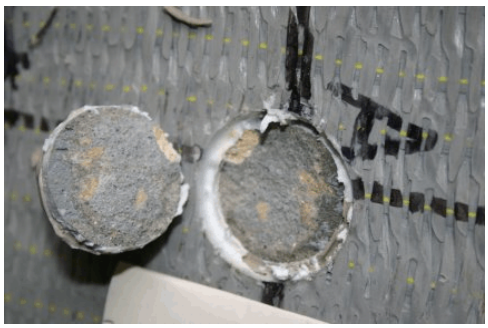

Figure A.75 F3 A Col 2 Row 3

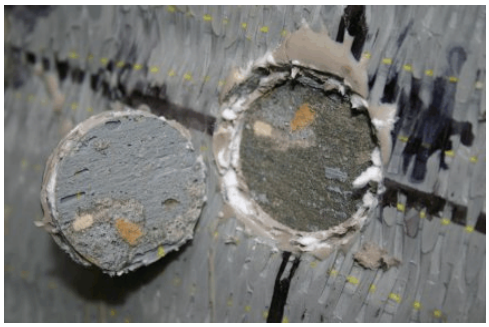

Figure A.76 F3 A Col 2 Row 4

Figure A.77 F3 A Col 3 Row 2

Figure A.78 F3 C Col 1 Row 6

Appendix A (Continued)

Figure A.79 F3 C Col 1 Row 10

Figure A.80 F3 A Col 3 Row 3

Figure A.81 F3 A Col 3 Row 4

Figure A.82 F3 A Col 3 Row 5

Figure A.83 F3 A Col 3 Row 6

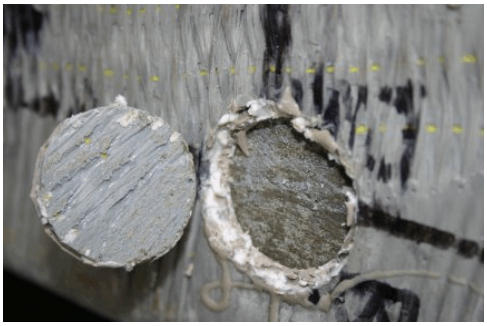

Figure A.84 F3 A Col 3 Row 7

Figure A.85 F3 A Col 3 Row 8

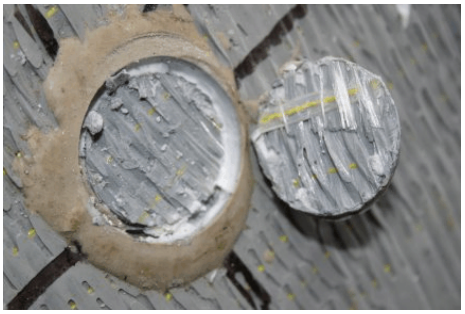

Figure A.86 F3 C Col 2 Row 4

Appendix A (Continued)

Figure A.87 F1 C Col 3 Row 3

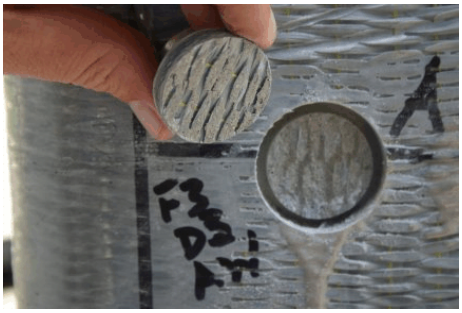

Figure A.88 F3 D Col 1 Row 3

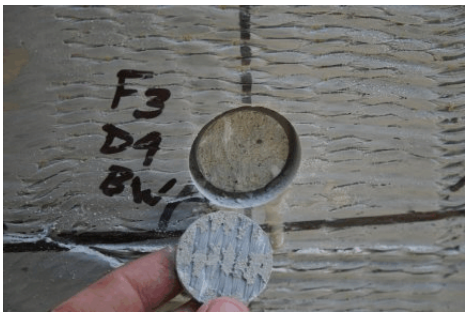

Figure A.89 F3 D Col 1 Row 9

Figure A.90 F3 D Col 2 Row 9

Figure A.91 F4 A Col 2 Row 9

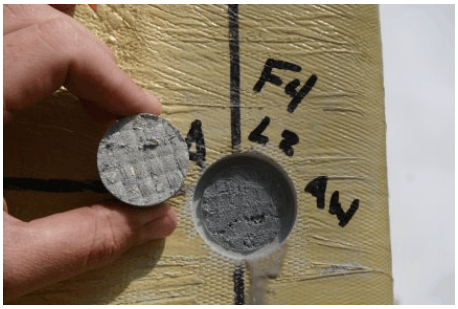

Figure A.92 F4 D Col 3 Row 2

Figure A.93 F2 C Col 1 Row 8

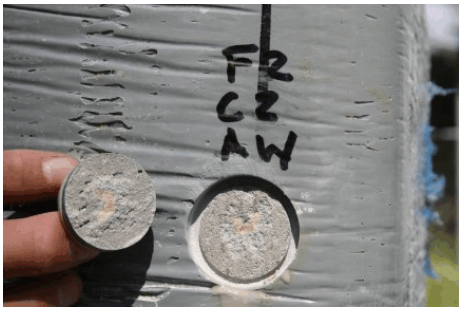

Figure A.94 F2 C Col 3 Row 2

Appendix A (Continued)

Figure A.95 F1 C Col 2 Row 7


Figure A.96 A1 C Col 1 Row 1

Figure A.97 A1 C Col 1 Row 2

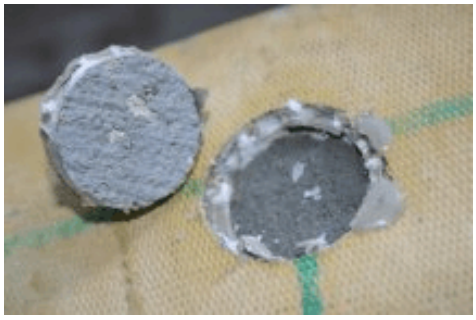
Figure A.98 A1 C Col 1 Row 4


Figure A.99 A1 C Col 2 Row 1

Figure A.100 A1 C Col 2 Row 2

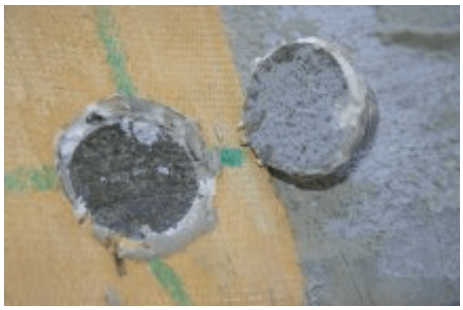
Figure A.101 A1 C Col 3 Row 1

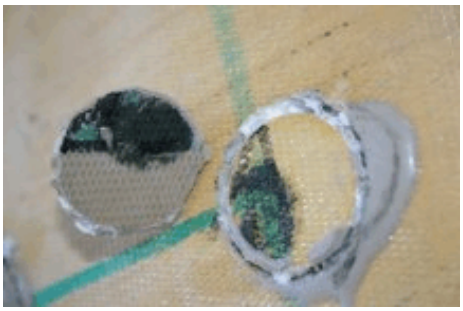
Figure A.102 A1 C Col 3 Row 2

Appendix A (Continued)

Figure A.103 A1 C Col 3 Row 3

Figure A.104 A1 C Col 3 Row 4

Figure A.105 A1 C Col 3 Row 8

Figure A.106 A3 B Col 1 Row 1

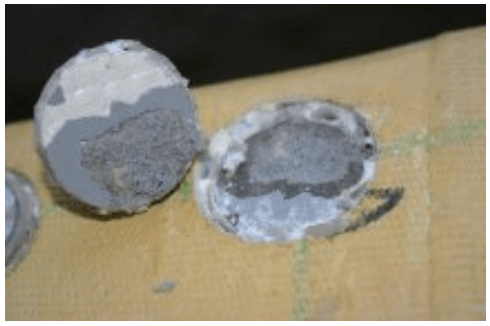

Figure A.107 A3 B Col 1 Row 4

Figure A.108 A3 B Col 1 Row 5

Figure A.109 A3 B Col 2 Row 1

Figure A.110 A3 B Col 2 Row 2

Appendix A (Continued)

Figure A.111 A3 B Col 2 Row 5

Figure A.112 A3 B Col 3 Row 1

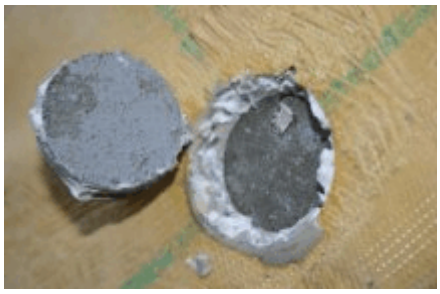

Figure A.113 A3 B Col 3 Row 2

Figure A.114 A3 B Col 3 Row 4

Figure A.115 A3 B Col 3 Row 5

Figure A.116 A4 A Col 1 Row 2

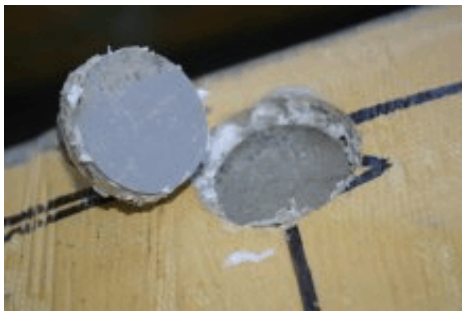

Figure A.117 A4 A Col 1 Row 3

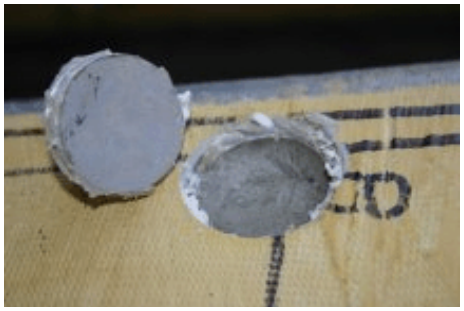

Figure A.118 A4 A Col 1 Row 5

Appendix A (Continued)

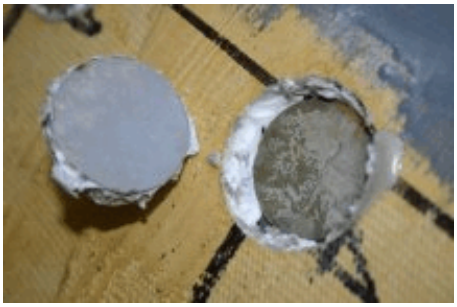

Figure A.119 A4 A Col 1 Row 8

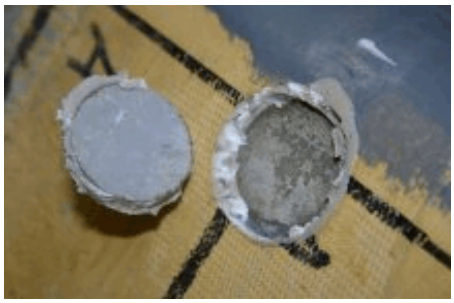

Figure A.120 A4 A Col 1 Row 9

Figure A.121 A4 A Col 2 Row 2

Figure A.122 A4 A Col 2 Row 3

Figure A.123 A4 A Col 2 Row 6

Figure A.124 A4 A Col 2 Row 7

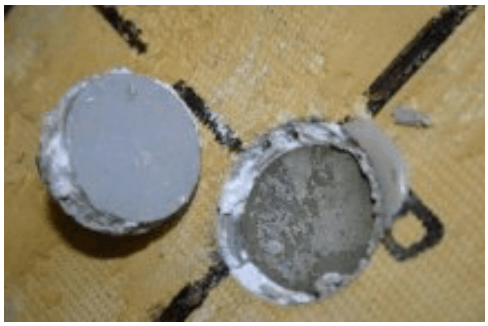

Figure A.125 A4 A Col 2 Row 9

Figure A.126 A4 A Col 3 Row 2

Appendix A (Continued)

Figure A.127 A4 A Col 3 Row 5

Figure A.128 A4 A Col 3 Row 6

Figure A.129 A4 A Col 3 Row 7

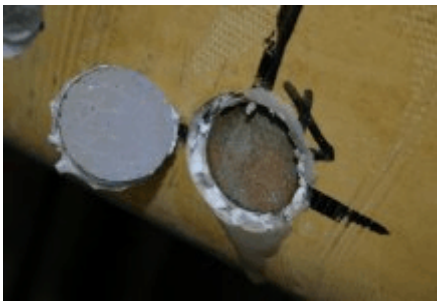

Figure A.130 A4 A Col 3 Row 8

Figure A.131 F4 A Col 1 Row 2

Figure A.132 F4 A Col 1 Row 3

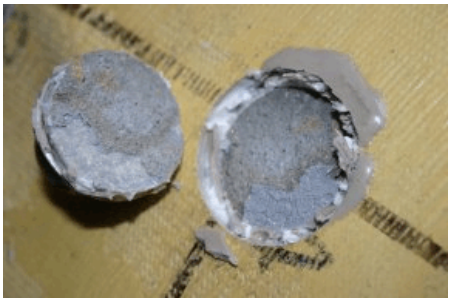

Figure A.133 F4 A Col 1 Row 4

Figure A.134 F4 A Col 1 Row 5

Appendix A (Continued)

Figure A.135 F4 A Col 1 Row 7

Figure A.136 F4 A Col 1 Row 8

Figure A.137 F4 A Col 1 Row 9

Figure A.138 F4 A Col 1 Row 10

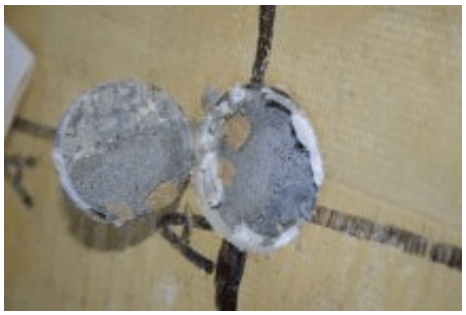

Figure A.139 F4 A Col 2 Row 2

Figure A.140 F4 A Col 2 Row 3

Figure A.141 F4 A Col 2 Row 4

Figure A.142 F4 A Col 2 Row 7

Appendix A (Continued)

Figure A.143 F4 A Col 2 row 10

Figure A.144 F4 A Col 3 Row 2

Figure A.145 F4 A Col 3 Row 3

Figure A.146 F4 A Col 3 Row 4

Figure A.147 F4 A Col 3 Row 6

Figure A.148 F4 A Col 3 Row 7

Figure A.149 F4 A Col 3 Row 8

Figure A.150 F4 A Col 3 Row 9

Appendix A (Continued)

Figure A.151 F4 A Col 3 Row 10

Appendix B Material Properties

B.1 Air Logistics System

The Aquawrap ® repair system uses a water-activated urethane resin and custom woven fabric that can be wrapped around the pile. Because it is water-activated the FRP material must be pre-impregnated with the resin and sent to the site in hermetically sealed foil pouches. The pouches are opened immediately prior to application in order to prevent premature curing due to atmospheric moisture. The properties of the uni-directional fibers and Aquawrap ® base primer #4, as well as those of Bio-Dur 563 epoxy are summarized in the following tables. All information was provided by the manufacturer.

Table B.1 Properties of Aquawrap ® Fabrics [4]

Properties	Quantities
Tensile Strength	85 ksi
Tensile Modulus	5200 ksi
Load per Ply	2400 lb/in

Table B.2 Properties of Aquawrap ® Base Primer #4 [4]

Properties	Quantities
Compressive Strength	10 ksi
Tensile Strength	4.8 ksi
Elongation at Break	40%
Flexural Strength	6.6 ksi
Shore Hardness	91

Appendix B (Continued)

Table B.3 Properties of Bio-Dur 563 [6]

Properties	Quantities
Compressive Strength	7.38 ksi
Tensile Strength	6.0 ksi
Flexural Strength	4.55 ksi

B.2 Fyfe System

Fyfe's Tyfo® SEH-51A is a custom-weave, uni-directional glass fabric that is usually used with Tyfo-S epoxy. However, for the underwater application Tyfo® SW-1 underwater epoxy was used. Because this is not water-activated it can be mixed at the site and the FRP fabric impregnated just prior to use. Material properties are provided by the manufacturer.

Table B.4 Properties of Tyfo ® SEH-51A Composite [5]

Properties	Quantities
Tensile Strength	3.3 k/in
Tensile Modulus	3030 ksi
Ultimate Elongation	2.2%
Laminate Thickness	0.05 in
Dry Fiber Weight per sq. yd.	27 oz.
Dry Fiber Thickness	0.014 in

Appendix B (Continued)

Table B.5 Properties of Tyfo ® SW-1 Epoxy [5]

Properties	Quantities
Compressive Strength (7 Day)	7-8 ksi
Specific Gravity	1.6
Mixing Ratio by Weight	100:56
Viscosity A&B (two components) Mixed	14000 - 18000 cps
Gel Time @ 65° F	2.5 - 3.5 hours

Appendix C Graphic Results Comparison

This section presents the findings for each pile, including visual, acoustic, thermographic analysis as well as pull-off testing, if applicable.

For the acoustic analysis, “A” = no hollowness detected, “B” = hollowness detected, delamination suspected, and “C”= obvious delamination.

For the thermographic analysis, a temperature of 97.5 ° F was taken to indicate delamination after comparison with the pull-off results. The scanning speed of the DEIT device was typically 1 in/sec. This varied slightly through different tests but the variability made only a negligible impact on the amount of heat energy distributed. The approximate scanning speeds are shown in Figure A.152.

Pull-off tests were not performed on all pile faces. For bond strength values on faces which did receive pull-off testing, values listed are in psi. Green indicates a satisfactory bond (>200 psi) while yellow indicates an unsatisfactory bond.

For the pull-off failure modes, green indicates a full concrete failure, yellow a partial concrete failure, red an FRP failure and white an epoxy failure. A small “x” indicates the area was not or could not be tested due to physical deformation of the FRP fabric. FC denotes a full concrete failure, PC a partial concrete failure, FRP a tensile fiber failure, VEIL a failure in the non-structural veil area, and EPX an epoxy failure.

Appendix C (Continued)

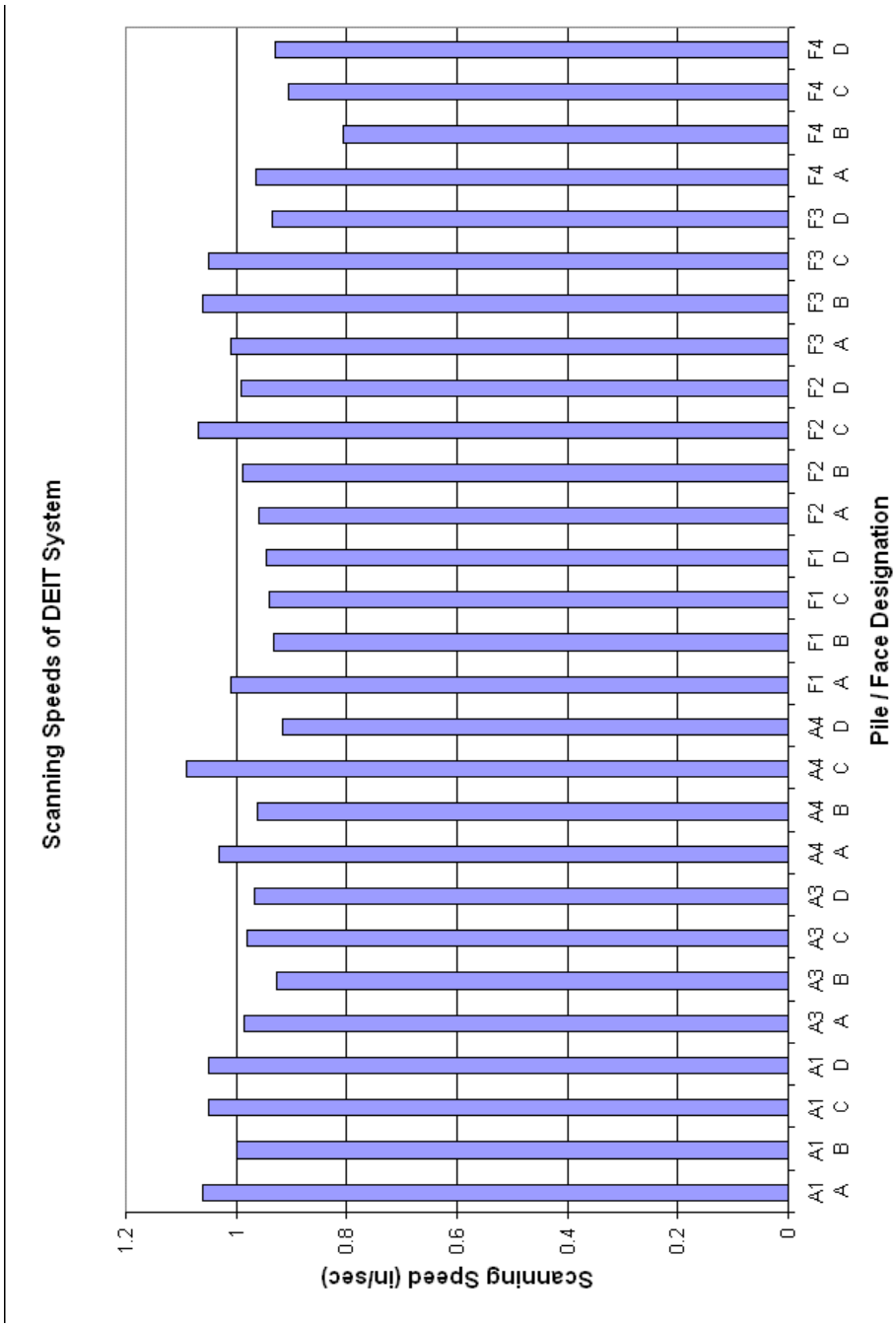

Figure C.1 Scanning Speeds of DEIT System

Appendix C (Continued)
Pile F1 Face A

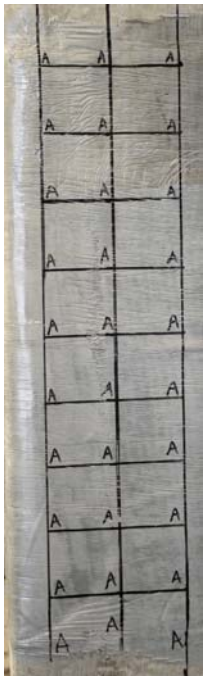

Figure C.2 Pile F1 Face A Color Photo

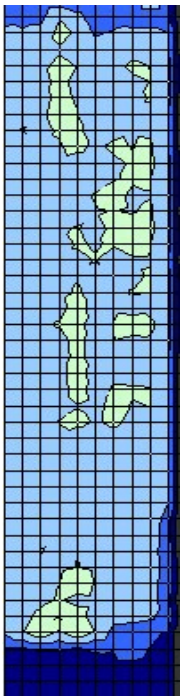

Figure C.3 Pile F1 Face A Thermal Scan

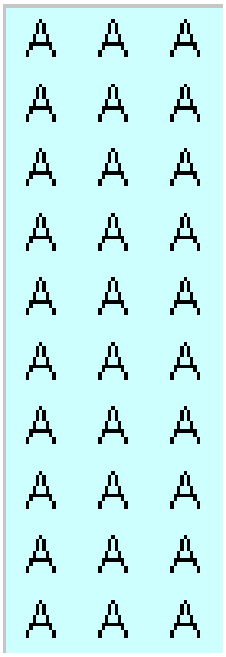

Figure C.4 Pile F1 Face A Acoustic Testing

Appendix C (Continued)
Pile F1 Face B

Figure C.5 Pile F1 Face B Color Photo

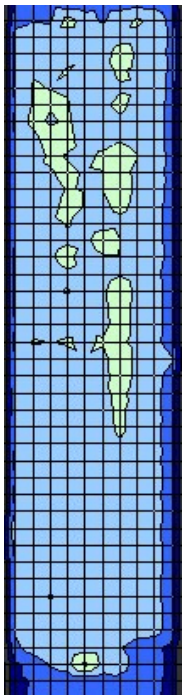

Figure C.6 Pile F1 Face B Thermal Scan

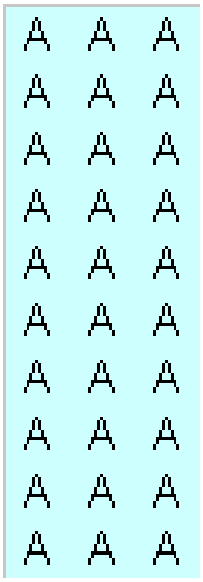

Figure C.7 Pile F1 Face B Acoustic Test

197	283	213
x	x	x
205	271	236
387	x	259
x	x	224
360	159	x
387	217	283
368	337	263
170	228	x
x	232	x

Figure C.8 Pile F1 Face B Pull-off Strength

FC	PC	FC
x	x	x
FC	FC	FC
FC	x	EP
x	x	FC
PC	FRP	x
PC	PC	FC
PC	PC	FC
FC	PC	x
x	PC	x

Figure C.9 Pile F1 Face B Pull-off Failure Mode

Appendix C (Continued)
Pile F1 Face C

Figure C.10
Pile F1 Face C
Color Photo

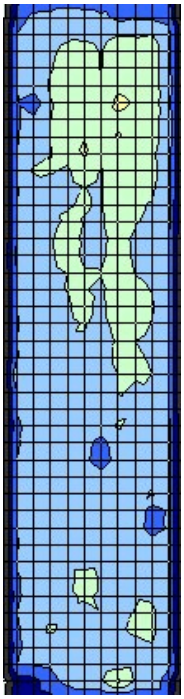

Figure C.11
Pile F1 Face
C Thermal
Scan

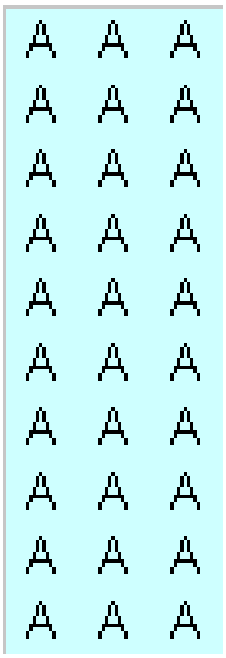

Figure C.12 Pile
F1 Face C
Acoustic Test

x	x	x
384	124	228
271	147	x
352	263	x
306	x	333
182	x	x
x	248	x
387	201	x
x	x	201
x	x	x

Figure C.13
Pile F1 Face
C Pull-off
Strength

x	x	x
FC	PC	PC
PC	PC	x
FC	FC	x
FC	x	PC
FC	x	x
x	PC	x
PC	PC	x
x	x	PC
x	x	x

Figure C.14
Pile F1 Face
C Pull-off
Failure
Mode

Appendix C (Continued)
Pile F1 Face D

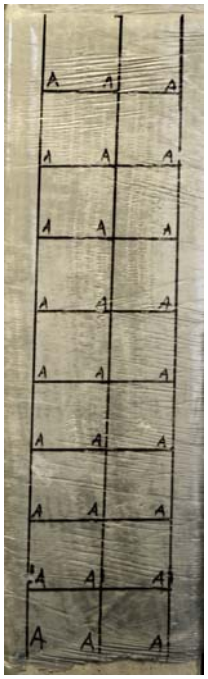

Figure C.15
Pile F1 Face D
Color Photo

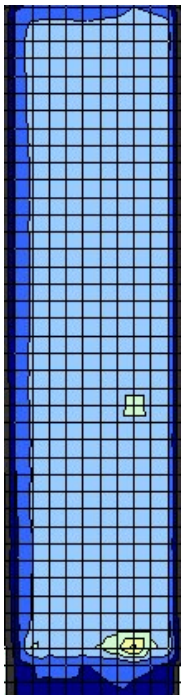

Figure C.16
Pile F1 Face
D Thermal
Scan

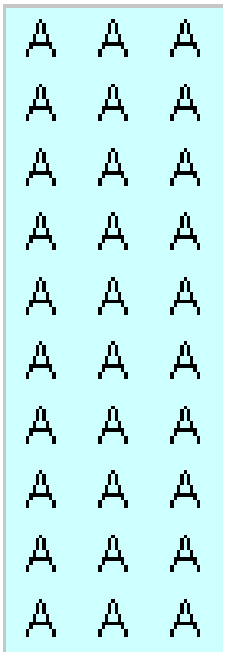

Figure C.17 Pile
F1 Face D
Acoustic Test

x	x	x
x	x	387
387	x	x
263	387	263
279	333	341
387	283	387
x	116	279
263	182	139
384	147	x
x	x	x

Figure C.18
Pile F1 Face
D Pull-off
Strength

x	x	x
x	x	FC
FC	x	x
FC	FC	FC
PC	PC	FC
FC	PC	FC
x	FRP	PC
PC	FRP	PC
PC	FRP	x
x	x	x

Figure C.19
Pile F1 Face
D Pull-off
Failure
Mode

Appendix C (Continued)
Pile F2 Face A

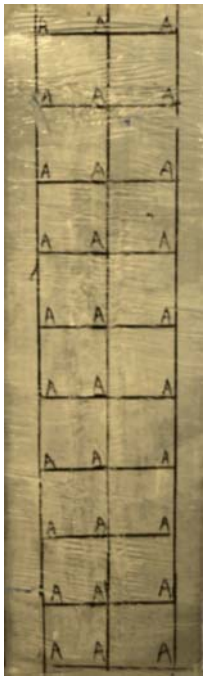

Figure C.20
Pile F2 Face A
Color Photo

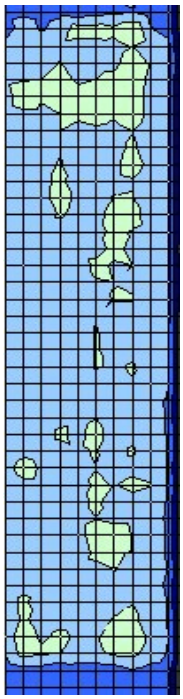

Figure C.21
Pile F2 Face
A Thermal
Scan

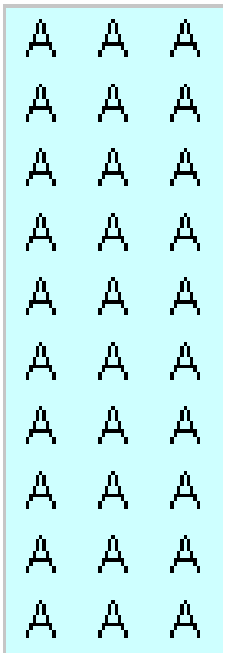

Figure C.22 Pile
F2 Face A
Acoustic Test

Appendix C (Continued)
Pile F2 Face B

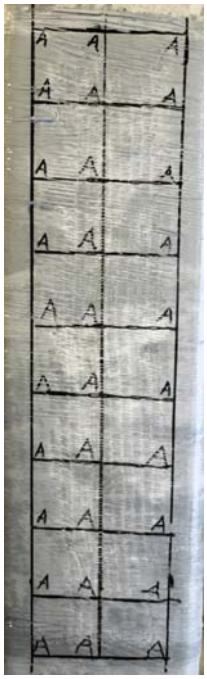

Figure C.23
Pile F2 Face B
Color Photo

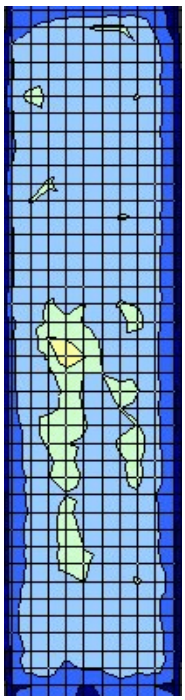

Figure C.24
Pile F2 Face
B Thermal
Scan

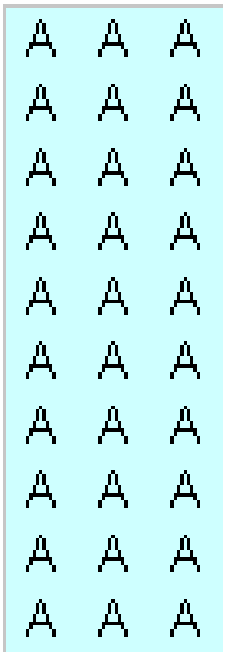

Figure C.25 Pile
F2 Face B
Acoustic Test

Appendix C (Continued)
Pile F2 Face C

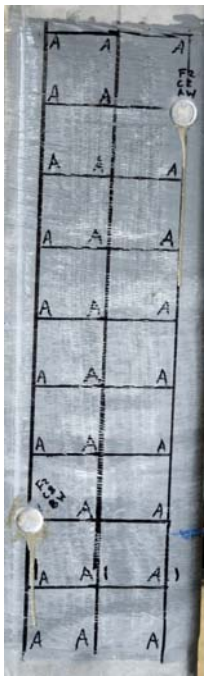

Figure C.26
Pile F2 Face C
Color Photo

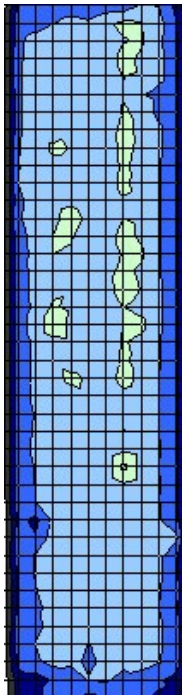

Figure C.27
Pile F2 Face
C Thermal
Scan

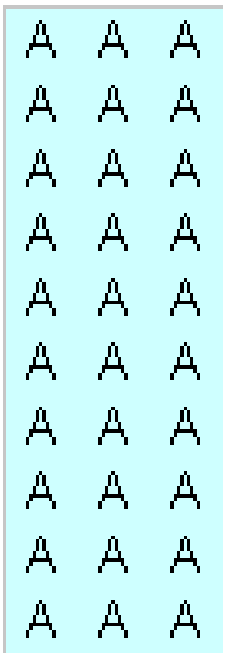

Figure C.28 Pile
F2 Face C
Acoustic Test

x	x	x
x	x	290
306	290	221
x	x	x
x	x	182
x	x	x
302	162	337
228	x	x
387	387	352
x	x	x

Figure C.29
Pile F2 Face
C Pull-off
Strength

x	x	FC
FC	FC	FC
x	x	x
x	x	PC
x	x	x
PC	PC	FRF
PC	x	x
FC	FC	PC
x	x	x

Figure C.30
Pile F2 Face
C Pull-off
Failure
Mode

Appendix C (Continued)
Pile F2 Face D

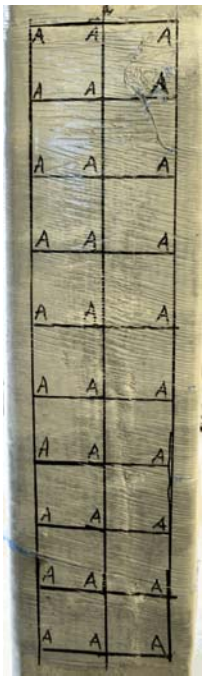

Figure C.31
Pile F2 Face D
Color Photo

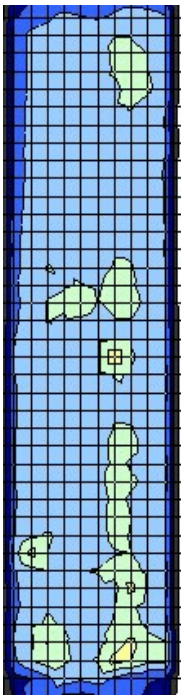

Figure C.32
Pile F2 Face
D Thermal
Scan

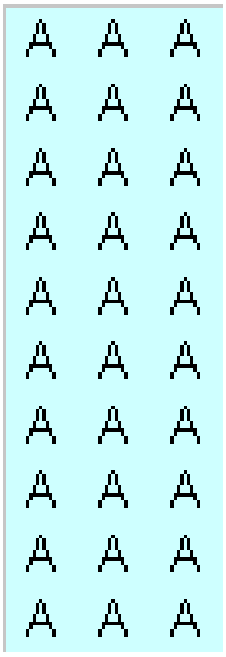

Figure C.33 Pile
F2 Face D
Acoustic Test

x	x	x
306	228	x
x	x	x
x	310	x
x	318	x
x	155	x
x	256	x
x	x	x
x	162	294
x	x	x

Figure C.34
Pile F2 Face
D Pull-off
Strength

x	x	x
PC	PC	x
x	x	x
x	FC	x
x	PC	x
x	PC	x
x	PC	x
x	x	x
x	PC	PC
x	x	

Figure C.35
Pile F2 Face
D Pull-off
Failure
Mode

Appendix C (Continued)
Pile F3 Face A

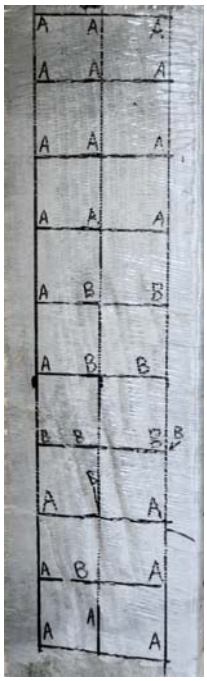

Figure C.36
Pile F3 Face A
Color Photo

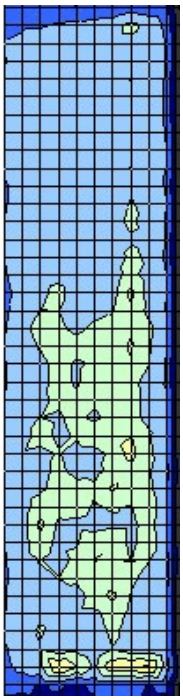

Figure C.37
Pile F3 Face
A Thermal
Scan

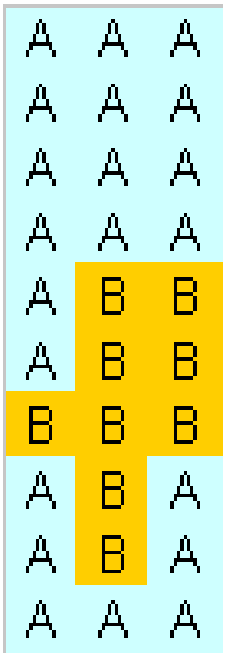

Figure C.38 Pile
F3 Face A
Acoustic Test

x	x	x
279	x	298
228	387	341
298	252	384
387	116	267
x	x	333
186	x	151
x	x	248
356	124	x
x	x	x

Figure C.39
Pile F3 Face
A Pull-off
Strength

x	x	x
FC	x	FC
FC	FC	FC
FC	PC	PC
FC	FRP	FC
x	x	PC
FRP	x	FRP
x	x	FRP
FC	FRP	x
x	x	x

Figure C.40
Pile F3 Face
A Pull-off
Failure
Mode

Appendix C (Continued)
Pile F3 Face B

Figure C.41
Pile F3 Face B
Color Photo

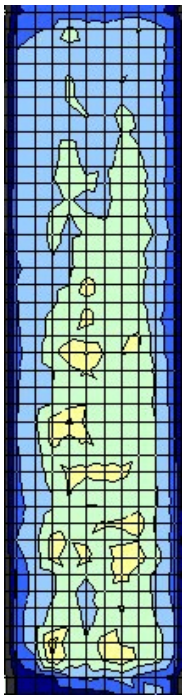

Figure C.42
Pile F3 Face
B Thermal
Scan

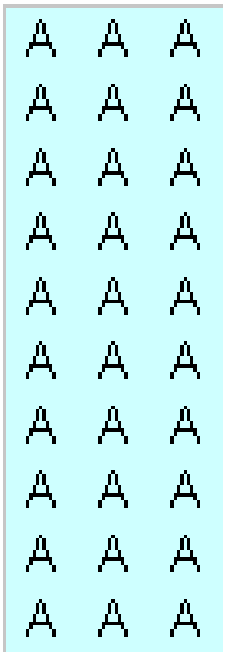

Figure C.43 Pile
F3 Face B
Acoustic Test

Appendix C (Continued)
Pile F3 Face C

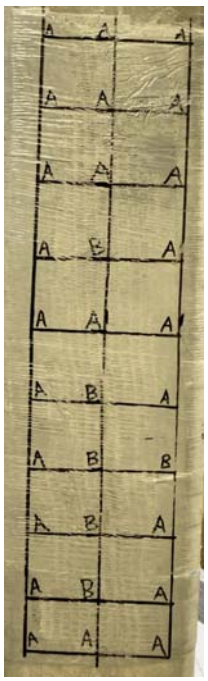

Figure C.44
Pile F3 Face C
Color Photo

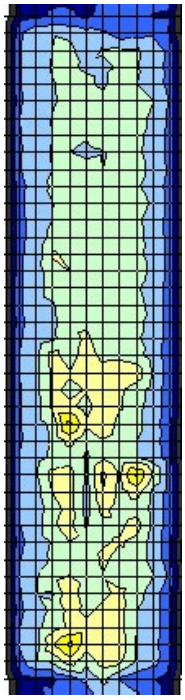

Figure C.45
Pile F3 Face
C Thermal
Scan

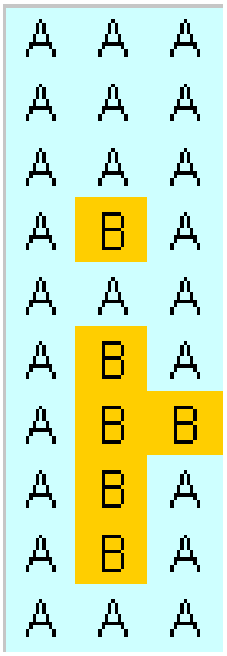

Figure C.46 Pile
F3 Face C
Acoustic Test

x	376	x
x	x	x
310	x	387
x	104	345
232	174	387
333	x	x
329	x	x
252	96	267
147	x	314
232	x	x

Figure C.47
Pile F3 Face
C Pull-off
Strength

x	PC	x
x	x	x
PC	x	PC
x	FRP	FC
PC	PC	FC
PC	x	x
PC	x	x
PC	PC	FC
PC	x	PC
PC	x	x

Figure C.48
Pile F3 Face
C Pull-off
Failure
Mode

Appendix C (Continued)
Pile F3 Face D

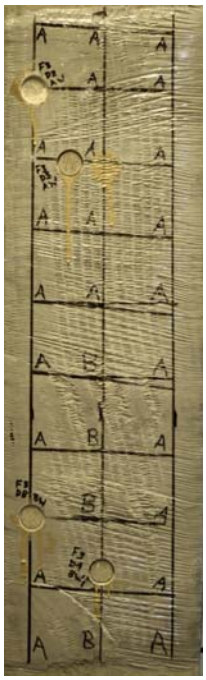

Figure C.49
Pile F3 Face D
Color Photo

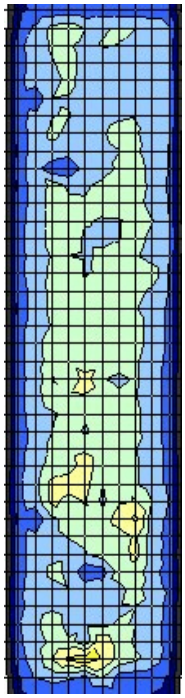

Figure C.50
Pile F3 Face
D Thermal
Scan

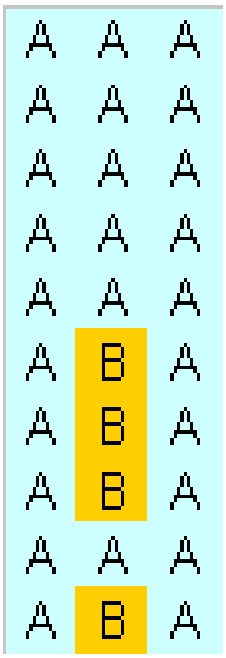

Figure C.51 Pile
F3 Face D
Acoustic Test

Appendix C (Continued)
Pile F4 Face A

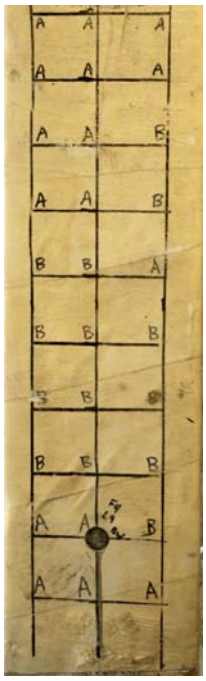

Figure C.52
Pile F4 Face A
Color Photo

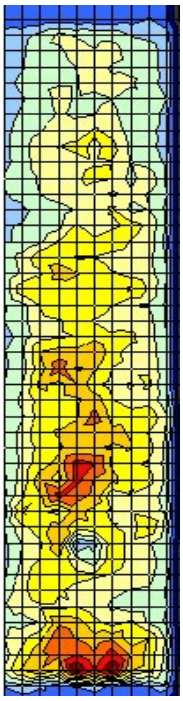

Figure C.53
Pile F4 Face
A Thermal
Scan

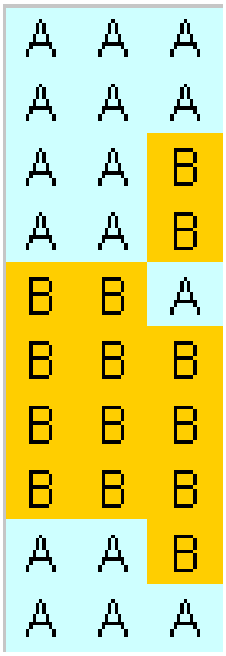

Figure C.54 Pile
F4 Face A
Acoustic Test

x	x	x
186	352	263
232	252	217
259	162	224
124	x	236
135	x	201
356	93	182
244	x	62
232	108	116
155	155	155

Figure C.55
Pile F4 Face
A Pull-off
Strength

x	x	x
PC	FC	PC
PC	FRP	FRP
PC	FRP	FRP
PC	x	FRP
FRP	x	FRP
FRP	VEIL	FRP
FRP	x	FRP
VEIL	PC	FRP
VEIL	FRP	FRP

Figure C.56
Pile F4 Face
A Pull-off
Failure
Mode

Appendix C (Continued)
Pile F4 Face B

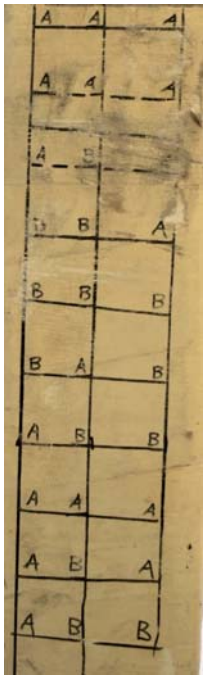

Figure C.57
Pile F4 Face B
Color Photo

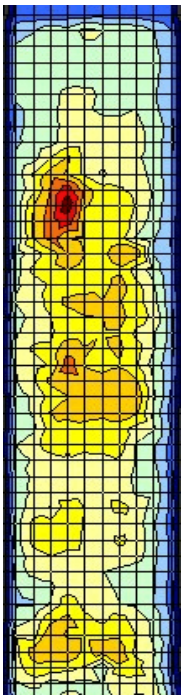

Figure C.58
Pile F4 Face
B Thermal
Scan

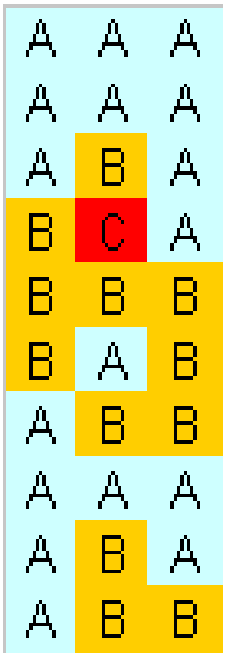

Figure C.59 Pile
F4 Face B
Acoustic Test

Appendix C (Continued)
Pile F4 Face C

Figure C.60
Pile F4 Face C
Color Photo

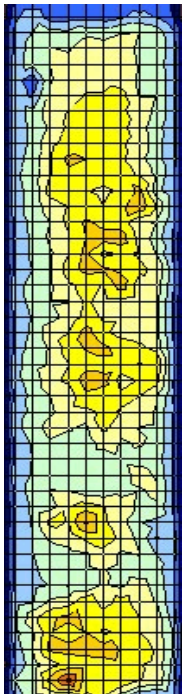

Figure C.61
Pile F4 Face
C Thermal
Scan

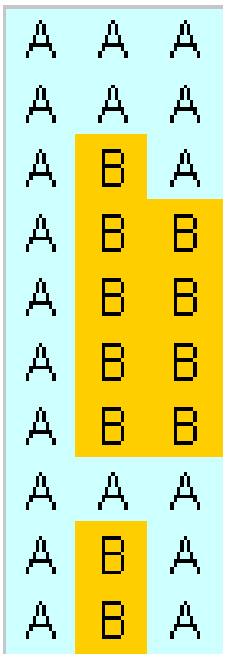

Figure C.62 Pile
F4 Face C
Acoustic Test

Appendix C (Continued)
Pile F4 Face D

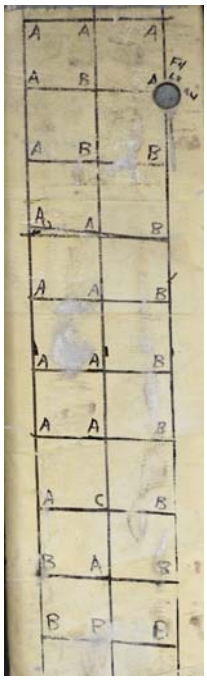

Figure C.63
Pile F4 Face D
Color Photo

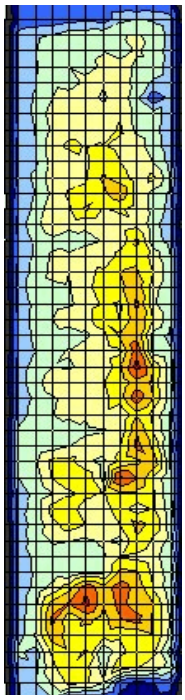

Figure C.64
Pile F4 Face
D Thermal
Scan

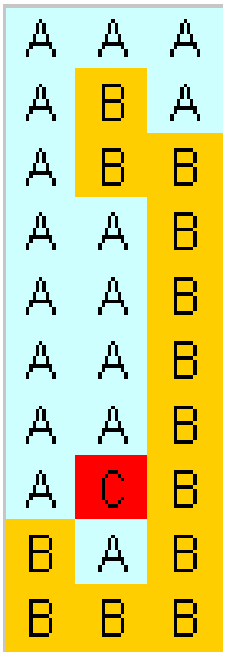

Figure C.65 Pile
F4 Face D
Acoustic Test

Appendix C (Continued)
Pile A1 Face A

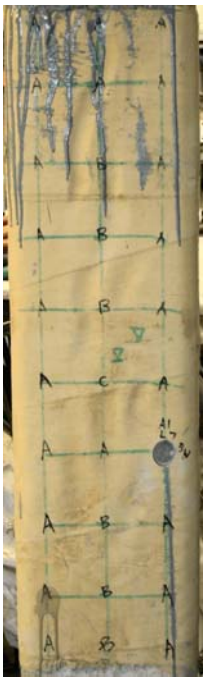

Figure C.66
Pile A1 Face A
Color Photo

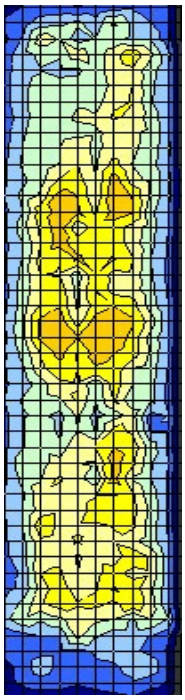

Figure C.67
Pile A1 Face
A Thermal
Scan

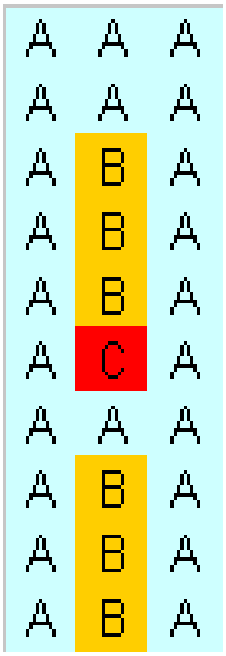

Figure C.68 Pile
A1 Face A
Acoustic Test

Appendix C (Continued)
Pile A1 Face B

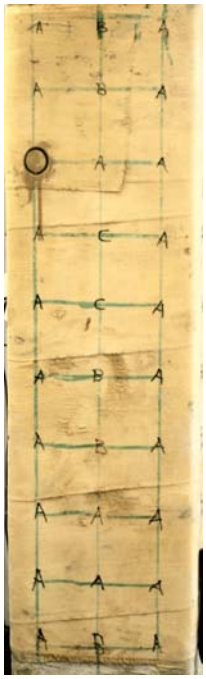

Figure C.69
Pile A1 Face B
Color Photo

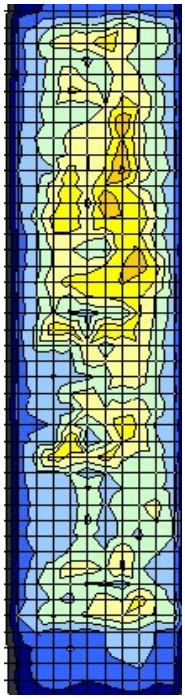

Figure C.70
Pile A1 Face
B Thermal
Scan

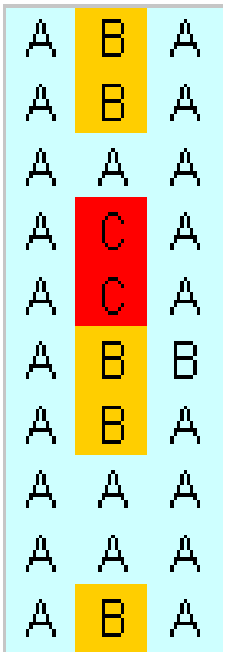

Figure C.71 Pile
A1 Face B
Acoustic Test

Appendix C (Continued)
Pile A1 Face C

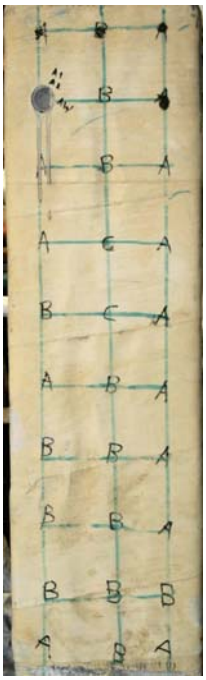

Figure C.72
Pile A1 Face C
Color Photo

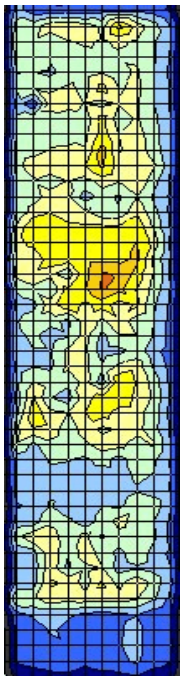

Figure C.73
Pile A1 Face
C Thermal
Scan

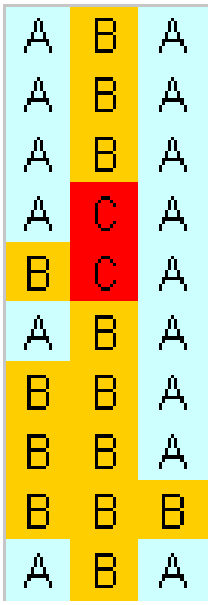

Figure C.74
Pile A1 Face C
Acoustic Test

x	19	197
77	19	236
x	x	162
38	x	306
x	x	x
0	x	0
x	0	x
0	x	77
x	0	x
0	x	0

Figure C.75
Pile A1 Face
C Pull-off
Strength

x	VEIL	FRP
PC	VEIL	EPX
x	x	PC
FRP	x	PC
x	x	x
x	x	x
x	x	x
x	x	FRP
x	x	x
x	x	x

Figure C.76
Pile A1 Face
C Pull-off
Failure
Mode

Appendix C (Continued)
Pile A1 Face D

Figure C.77
Pile A1 Face D
Color Photo

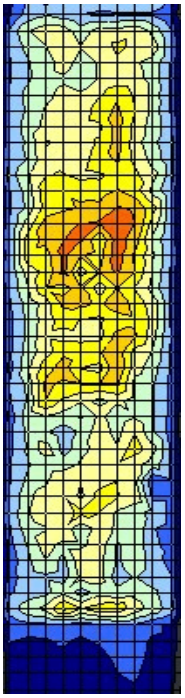

Figure C.78
Pile A1 Face
D Thermal
Scan

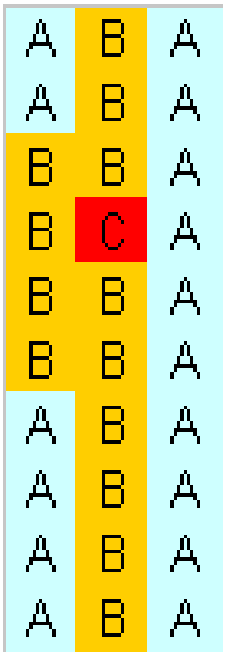

Figure C.79 Pile
A1 Face D
Acoustic Test

x	x	x
228	96	190
x	x	197
116	x	178
62	x	69
85	62	x
147	58	x
38	73	50
54	46	54
x	x	x

Figure C.80
Pile A1 Face
D Pull-off
Strength

x	x	x
FRP	VEIL	FRP
x	x	FRP
FRP	x	FRP
FRP	x	FRP
FRP	FRP	x
FRP	FRP	x
FRP	FRP	FRP
FRP	FRP	FRP
x	x	x

Figure C.81
Pile A1 Face
D Pull-off
Failure
Mode

Appendix C (Continued)
Pile A3 Face A

Figure C.82
Pile A3 Face A
Color Photo

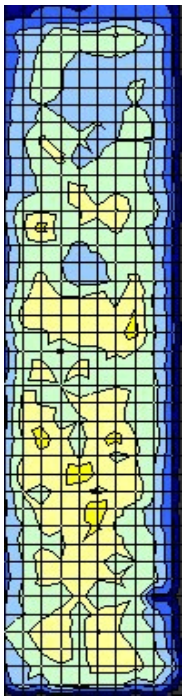

Figure C.83
Pile A3 Face
A Thermal
Scan

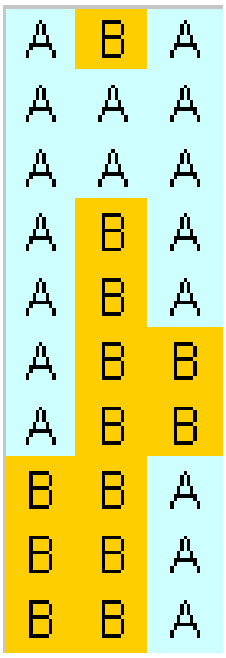

Figure C.84 Pile
A3 Face A
Acoustic Test

x	x	x
124	116	108
209	85	128
50	89	81
58	54	124
x	0	x
0	x	0
x	0	x
0	x	0
x	0	x

Figure C.85
Pile A3 Face
A Pull-off
Strength

x	x	x
FRP	PC	FC
FRP	VEIL	PC
FRP	FRP	FRP
VEIL	FRP	FRP
x	x	x
x	x	x
x	x	x
x	x	x
x	x	x

Figure C.86
Pile A3 Face
A Pull-off
Failure
Mode

Appendix C (Continued)
Pile A3 Face B

Figure C.87
Pile A3 Face B
Color Photo

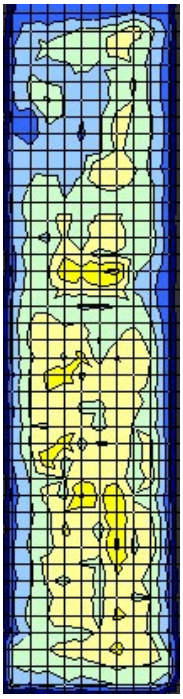

Figure C.88
Pile A3 Face
B Thermal
Scan

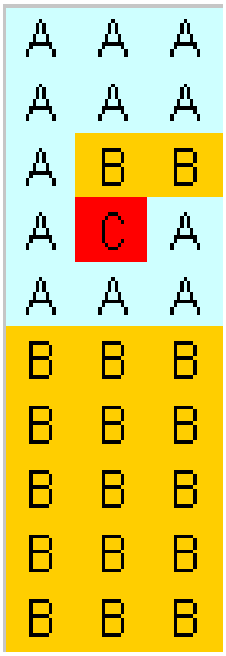

Figure C.89 Pile
A3 Face B
Acoustic Test

116	135	387
256	120	248
x	x	x
197	x	50
139	77	166
0	x	0
x	0	x
0	x	0
x	0	x
0	x	0

Figure C.90
Pile A3 Face
B Pull-off
Strength

FRP	EPX	FRP
PC	VEIL	PC
x	x	x
PC	x	FRP
VEIL	FRP	FRP
x	x	x
x	x	x
x	x	x
x	x	x
x	x	x

Figure C.91
Pile A3 Face
B Pull-off
Failure
Mode

Appendix C (Continued)
Pile A3 Face C

Figure C.92
Pile A3 Face C
Color Photo

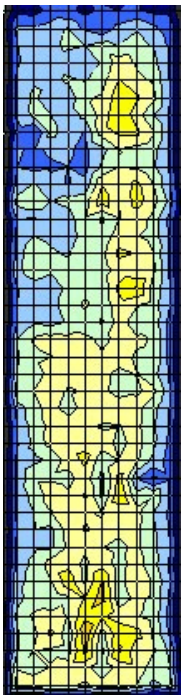

Figure C.93
Pile A3 Face
C Thermal
Scan

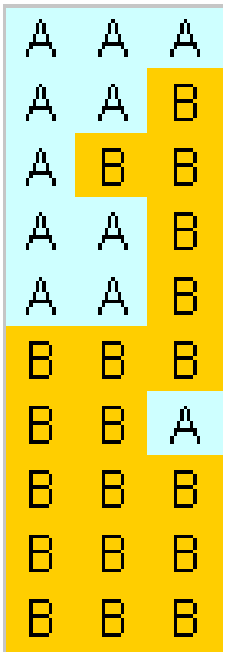

Figure C.94 Pile
A3 Face C
Acoustic Test

Appendix C (Continued)
Pile A3 Face D

Figure C.95
Pile A3 Face D
Color Photo

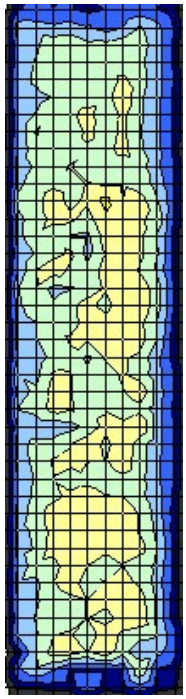

Figure C.96
Pile A3 Face
D Thermal
Scan

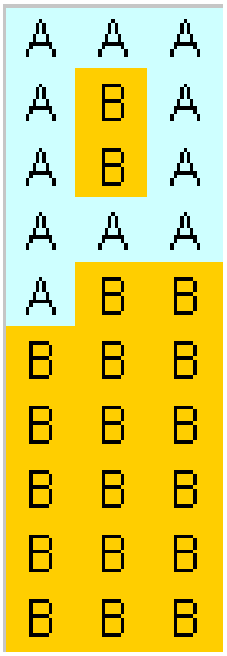

Figure C.97 Pile
A3 Face D
Acoustic Test

Appendix C (Continued)
Pile A4 Face A

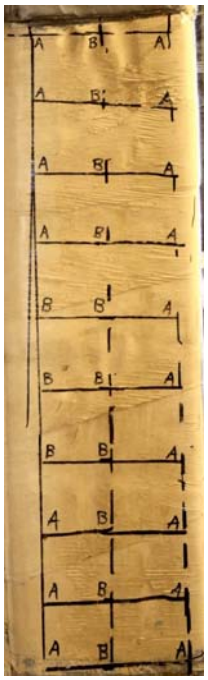

Figure C.98
Pile A4 Face A
Color Photo

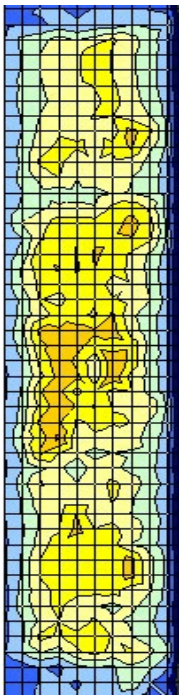

Figure C.99
Pile A4 Face
A Thermal
Scan

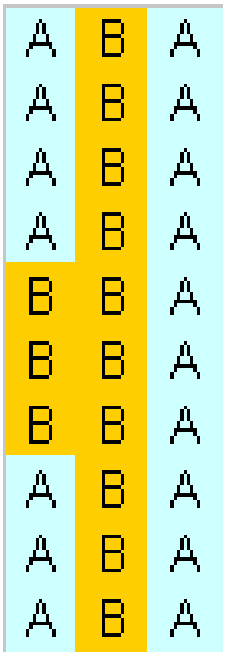

Figure C.100
Pile A4 Face A
Acoustic Test

x	x	x
252	85	368
124	58	x
x	x	x
85	x	116
x	65	100
85	54	89
77	x	77
108	58	x
x	x	x

Figure C.101
Pile A4 Face
A Pull-off
Strength

x	x	x
FRP	FRP	PC
FRP	VEIL	x
x	x	x
FRP	x	FRP
x	VEIL	FRP
FRP	FRP	FRP
FRP	x	FRP
FRP	FRP	
x	x	x

Figure C.102
Pile A4 Face
A Pull-off
Failure
Mode

Appendix C (Continued)
Pile A4 Face B

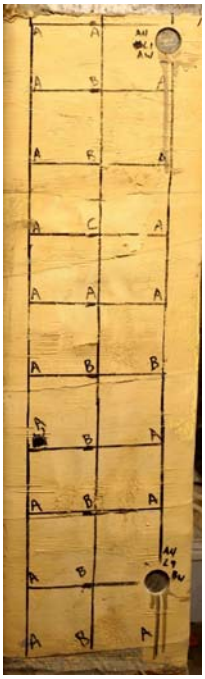

Figure C.103
Pile A4 Face B
Color Photo

Figure C.104
Pile A4 Face
B Thermal
Scan

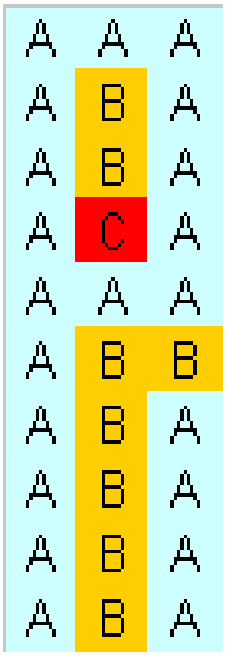

Figure C.105
Pile A4 Face B
Acoustic Test

Appendix C (Continued)
Pile A4 Face C

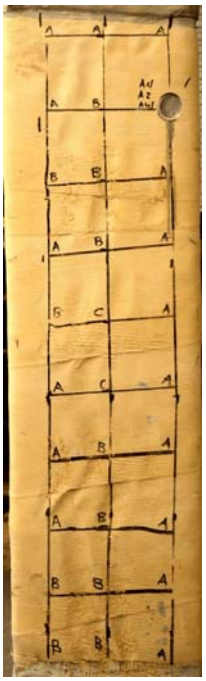

Figure C.106
Pile A4 Face C
Color Photo

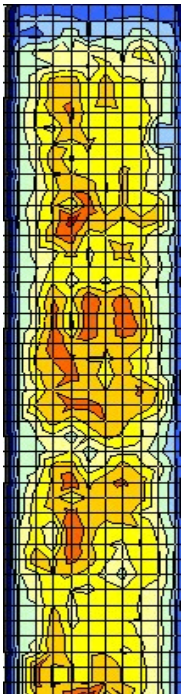

Figure C.107
Pile A4 Face
C Thermal
Scan

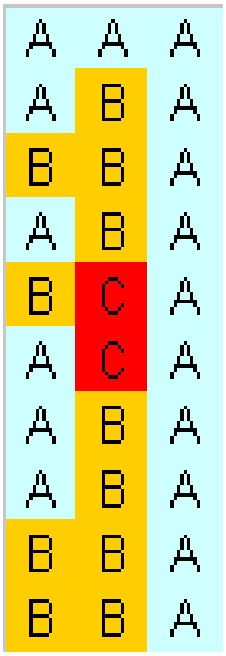

Figure C.108
Pile A4 Face C
Acoustic Test

Appendix C (Continued)
Pile A4 Face D

Figure C.109
Pile A4 Face D
Color Photo

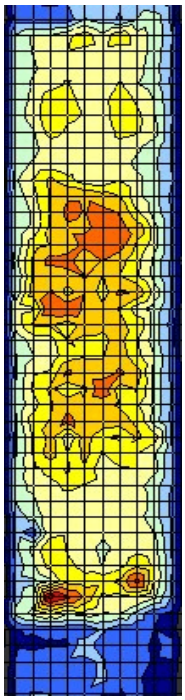

Figure C.110
Pile A4 Face
D Thermal
Scan

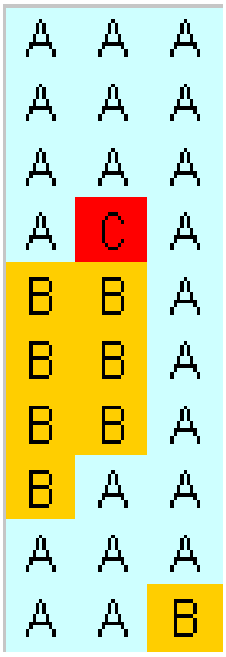

Figure C.111
Pile A4 Face D
Acoustic Test